UNCLASSIFIED

AD NUMBER
ADB262630

NEW LIMITATION CHANGE

TO

Approved for public release, distribution unlimited

FROM

Distribution authorized to U.S. Gov't. agencies only; Proprietary Info.; Sep 99. Other requests shall be referred to U.S. Army Medical Research and Materiel Command, 504 Scott St., Fort Detrick, MD 21702-5012.

AUTHORITY

U.S. Army Medical Research and Materiel Command and Fort Detrick ltr., dtd October 17, 2001.

THIS PAGE IS UNCLASSIFIED

AD_____

Award Number: DAMD17-96-C-6061

TITLE: 3-D Ultrasound Vascularity Assessment for Breast Cancer
       Diagnosis

PRINCIPAL INVESTIGATOR: Paul L. Carson, Ph.D.

CONTRACTING ORGANIZATION: University of Michigan
                          Ann Arbor, Michigan 48109-1274

REPORT DATE: September 1999

TYPE OF REPORT: Annual

PREPARED FOR: U.S. Army Medical Research and Materiel Command
               Fort Detrick, Maryland 21702-5012

20010124 019

NOTICE

THIS TECHNICAL REPORT HAS BEEN REVIEWED AND IS APPROVED FOR PUBLICATION.

_____   _____

N̶ṃ̶ṛ̶ỵ̶ (signature) 12/22/c̶   _____

REPORT DOCUMENTATION PAGE

Form Approved
OMB No. 0704-0188

1. AGENCY USE ONLY (Leave blank)	2. REPORT DATE September 1999	3. REPORT TYPE AND DATES COVERED Annual (1 Sep 98 – 31 Aug 99)

4. TITLE AND SUBTITLE
3-D Ultrasound Vascularity Assessment for Breast Cancer Diagnosis

5. FUNDING NUMBERS
DAMD17-96-C-6061

6. AUTHOR(S)
Paul L. Carson, Ph.D.

7. PERFORMING ORGANIZATION NAME(S) AND ADDRESS(ES)
University of Michigan
Ann Arbor, Michigan 48109-1274

E-Mail:
pcarson@umich.edu

8. PERFORMING ORGANIZATION REPORT NUMBER

9. SPONSORING/MONITORING AGENCY NAME(S) AND ADDRESS(ES)
Commander
U.S. Army Medical Research and Materiel Command
Fort Detrick, Frederick, Maryland 21702-5012

10. SPONSORING/MONITORING AGENCY REPORT NUMBER

11. SUPPLEMENTARY NOTES

This report contains colored photos

12a. DISTRIBUTION / AVAILABILITY STATEMENT

Distribution authorized to U.S. Government agencies only
(proprietary information, Sep 99). Other requests for this
document shall be referred to U.S. Army Medical Research and
Materiel Command, 504 Scott Street, Fort Detrick, Maryland 21702-5012.

12b. DISTRIBUTION CODE

13. ABSTRACT (Maximum 200

This project is to improve the diagnosis and management of patients with breast cancer through development and evaluation of 3D ultrasound imaging and quantification techniques emphasizing vascularity. Progress this second year included advances which should increase the sensitivity and specificity of ultrasound imaging in discriminating benign from malignant known masses. Preliminary data analyses were completed on new trials and contributions were made to advance 3D image acquisition, display and quantification. The registration achieved so far in compound and sequential imaging is unexpectedly good and robust. It has promise for an increasing number of applications that could revolutionize the use of ultrasound in medicine, particularly for serial studies. Our new extended 3D field of view imaging appears to greatly increase the changes of achieving these goals. The results to date in image-based slice positioning continue to be impressive, and at least two companies have implemented aspects of the technique, one with clear acknowledgement of our developments. 3D detection and display of lactic ducts has been illustrated in concept, but much more work will be required to show practical, routine utility.

14. SUBJECT TERMS Breast Cancer			15. NUMBER OF PAGES 61
			16. PRICE CODE

17. SECURITY CLASSIFICATION OF REPORT Unclassified	18. SECURITY CLASSIFICATION OF THIS PAGE Unclassified	19. SECURITY CLASSIFICATION OF ABSTRACT Unclassified	20. LIMITATION OF ABSTRACT Limited

FOREWORD

Opinions, interpretations, conclusions and recommendations are those of the author and are not necessarily endorsed by the U.S. Army.

_X__ Where copyrighted material is quoted, permission has been obtained to use such material.

_X__ Where material from documents designated for limited distribution is quoted, permission has been obtained to use the material.

__X_ Citations of commercial organizations and trade names in this report do not constitute an official Department of Army endorsement or approval of the products or services of these organizations.

N/A In conducting research using animals, the investigator(s) adhered to the "Guide for the Care and Use of Laboratory Animals," prepared by the Committee on Care and use of Laboratory Animals of the Institute of Laboratory Resources, national Research Council (NIH Publication No. 86-23, Revised 1985).

X_ For the protection of human subjects, the investigator(s) adhered to policies of applicable Federal Law 45 CFR 46.

N/A In conducting research utilizing recombinant DNA technology, the investigator(s) adhered to current guidelines promulgated by the National Institutes of Health.

N/A In the conduct of research utilizing recombinant DNA, the investigator(s) adhered to the NIH Guidelines for Research Involving Recombinant DNA Molecules.

N/A In the conduct of research involving hazardous organisms, the investigator(s) adhered to the CDC-NIH Guide for Biosafety in Microbiological and Biomedical Laboratories.

_____   11/15/99
PI - Signature   Date

I. TABLE OF CONTENTS

STANDARD FORM (SF) 298

FOREWORD

II. INTRODUCTION

The research to be conducted over the four year period of this contract centers around three areas 1) expansion of clinical trials capabilities performed under an ongoing NIH grant and their continuation after those trials are completed; 2) image registration using the mutual information cost function for evaluation/demonstration of image compounding and sequential examinations; 3) approaches to real time image-based slice positioning; 4) the, as yet, unique effort to image lactic ducts in 3D and perform preliminary evaluation of their diagnostic potential. Most of the research will be performed in parallel by various investigators. The following time line for the third and fourth years was given in the funded scope of work.

Table 1. Time Line for Present and Next Project Periods	Year 3	Year 4
Clinical Trials		
Validation/improvement of vascularity measures		
Clinical Trials of ~30 subjects	- + - +	+ +
Trials data analysis and write-up		+ +
Compound and Sequential Imaging		
Develop automated image registration by mutual information	+ - + -	+ + + +
Process ultrasound images to evaluate/demonstrate compound and sequential* imaging therewith		+
Image-based Slice Positioning [IBaR]		
Real time speckle decorrelation for image plane positioning	- +	- + - -
Digital ductography development	+ +	
Ductographic analysis of selected clinical trial cases	+ +	- +

*Auto registration of breast images from multiple exams   + = concentrated effort   - = modest effort

The following series of deliverables and associated materials are included in this annual progress report. Included are a listing of papers, abstracts and manuscripts, published and submitted.

Year 03
Item 1:   Summary report of clinical trials conducted and analyzed in the third year.
Item 2:   Summary report on initial real-time implementation of IBaR.
Item 3:   Interim report on ductography techniques.

IV. BODY
Progress has been made in the four areas of emphasis of this grant as listed below.

A. Clinical Trials and Vascularity Measures

1. Clinical Trials of ~30 subjects (Deliverable Item 1.)
We have studied 7 subjects, using the latest apparatus including the 1.5 D matrix array scanhead for discrimination of benign and malignant breast masses and evaluation of 3D compound imaging. Some of the competing grants are winding down and the rate will accelerate in year 04.

2. Trials data analysis and write-up
This contract contributed to a publication and a poster on clinical trials methods and preliminary results, References/Appendices 1 and 5, and to a more complete clinical trials results publication about to

be submitted. Some of the outstanding results from that analysis of quantitative 3D color flow imaging for breast cancer discrimination are shown in Figure 1.

B. Compound and Sequential Imaging

Because of our exciting advances with the automatic registration of two or more 3D image sets for assessment of sequential and compound imaging, we have continued to emphasize this goal during year 03 and the tasks for this year have been met fully. The surprising high resolution and improvement in detectability of low contrast regions and connective tissue layers are revealed in Figure 2.

1. Develop automated image registration by mutual information

The software developed here, MIAMI Fuse, continues to be refined and its utility for application to diagnostic ultrasound extended. The first demonstrated 3D coregistrations of ultrasound image sets were published in Reference/Appendix 2.

2. Process ultrasound images to evaluate/demonstrate compound and sequential* imaging therewith

The software has been modified and the registration is now being applied on patient examples for demonstration of each of several uses, including: 1) tracking changes for patients undergoing chemotherapy and antiangiogenesis therapy (References/Appendices 2&3); 2) highlighting and quantifying changes in essentially normal breasts as a prelude to improved detection of preclinical disease; 3) combining 3D data sets from various ultrasound imaging modes to properly register the unique information provided by each (References/Appendices 2&3); 4) expanding the field of view by combining several partially-overlapping 3D scans to see the full volume of medium to large lesions and reasonable amounts of surrounding vascular morphology and to show a reasonable volume of the breast for tracking difficult areas of the breast in follow up studies (Reference/Appendix 3); 5) combining views from multiple angles (compounding) (Reference/Appendix 4). In this year the compounding examples have been added to the list of outstanding results, although more work is needed to address the effects of some artifacts.

C. Image-based Registration of Slice Position [IBaR]

1. Real time speckle decorrelation for image plane positioning (Deliverable Item 2.)

As part of our research on this topic, we have continued to work formally with one company and informally with another, both of which have implemented crude real time versions of our IBaR technology (Reference 7). One has implemented software which uses the image decorrelation to estimate the average scan rate over the entire 3D sweep and applies that average rate to assign the image slice spacings. The other does not appear yet to apply the true decorrelation calculation on the clinically-released systems. To accurately estimate elevational movement, the frame rates must be high enough such that consecutive images are not completely decorrelated. We have arranged availability of a state of the art scanner for full time research that has the real time frame rates (often used in echocardiography) that are required for more successful measurement of scan distances at normal scan rates.

D. Digital ductography development

Software tools were developed in the previous year to help the user manually find, map and review ductal structures in the volume of B mode ultrasound data. Initially, the user identifies the relative location of the nipple to the data volume. The user then searches the volume by rotating a plane about the nipple. When a duct-like structure is seen, the user draws a line along the duct. The software then enables him to rotate the search plane around this line to verify if it is a duct, find the portions of it not in the initial search plane, and identify visible lobules feeding it. During this process, the user can mark any feature as part of the ductal tree, ultimately creating a 3D mapping of ductal structures within the volume.

1. Ductographic analysis of selected clinical trial cases (Deliverable Item 3.)

These graphical analysis tools have proven useful for visual development and for touchup of automated duct definition in a few selected cases. The main work will be in more automated duct

3

development, which has not been undertaken extensively due to the major emphasis we have placed on the compound imaging.

We have developed, in conjunction with CIRS, Inc., a phantom that can be used for many purposes, including testing of detection and delineation of short lengths of ducts. This CIRS Model 44 cylindrical plug phantom is shown in Figure 4. It contains 45, high contrast stubby cylinders within the imaging range of the M12 scanhead planned for this study. These are in known locations relative to each other for tests of spatial registration accuracy in multiple view compounding, as well as for the ductographic detection. This and any other phantoms can be used in combination with the beam aberrating plate (Figure 3) to produce the degraded image quality found in breast imaging.

E.   Figures
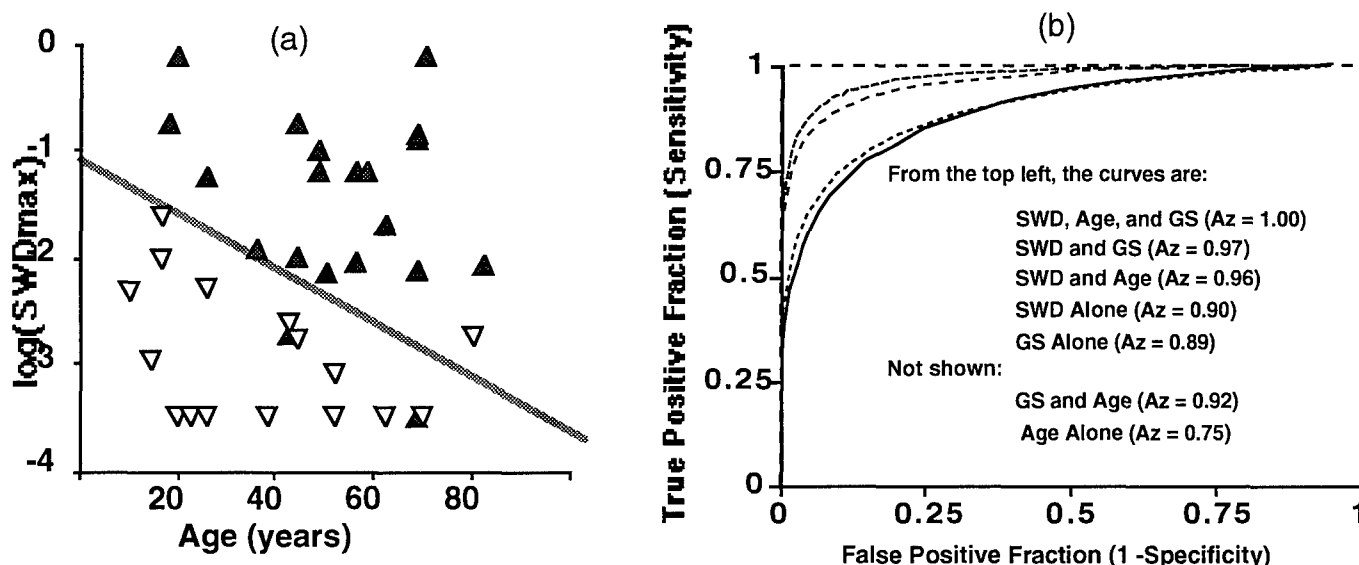
Figure 1. (a) Discrimination of benign (open triangles) and malignant (shaded triangles) breast tumors for 38 cases studied: 18 benign (mean age 46), 20 malignant (mean age 56). (b) Discrimination Index including one subjective measure, grayscale rating. Points are spread horizontally for clarity. (c) ROC curves for various combinations of SWD, age, and average gray scale (GS) rating. From worst to best performance, the criteria ranked (5) GS alone, (4) SWD alone, (3) SWD combined with age, (2) SWD combined with GS, and (1) the combined SWD-Age-GS Index, providing %100 discrimination in this 38 patient population.
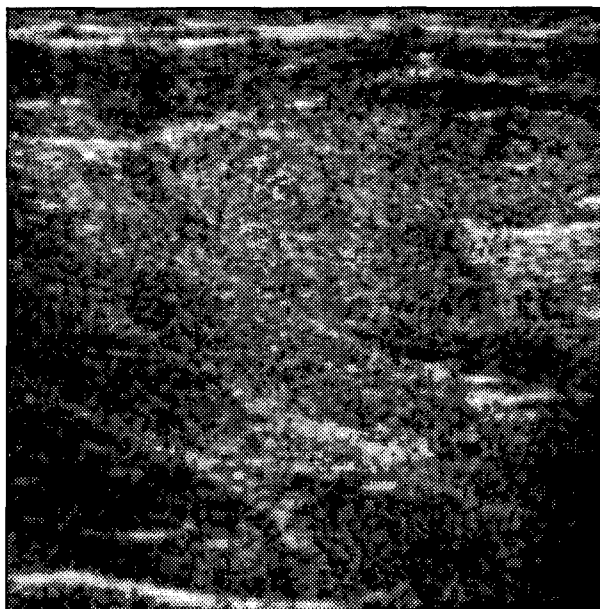
Figure 2. *(a) Uncompounded image of a breast from reference, 0° scan. Statistical analysis showed an almost ideal* $\propto \sqrt{N}$ *increase in SNR and CNR (contrast-to-noise ratio) for N views compounded vs. this reference view. Note the overall reduction in granularity and the better delineation of connective tissues (gray arrow) in (b).*

(b) Same image area compounded from 5 scans at 0°, 6.4°, 12.8°, -5.1°, and −10.2°, registered using 11 control point warping transformations. Most importantly, note the slightly hypoechoic, lobulated inhomogeneities surrounding the left end of the hyperechoic structure on the central right. The white arrow denotes one such lobulation with a thin, echogenic rim that is not visible on any of the constituent single views.
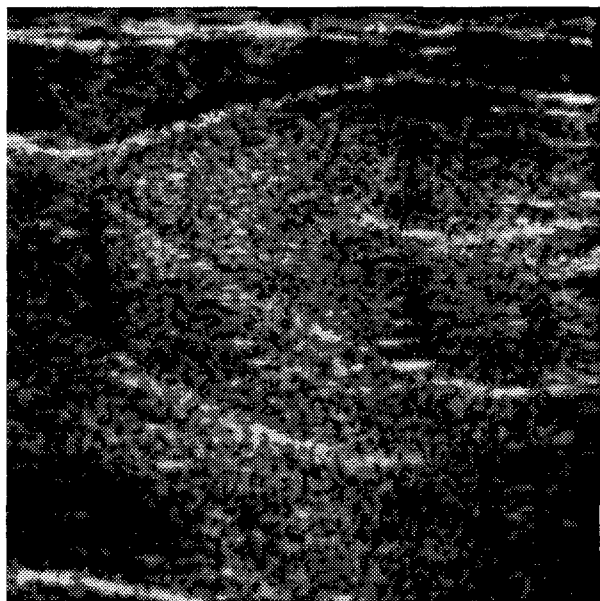
(c) Uncompounded image of a breast from reference, 0°, scan, 2.4 mm (8 slices) superior to image (a). Structures noted in (d) are not seen as well here.
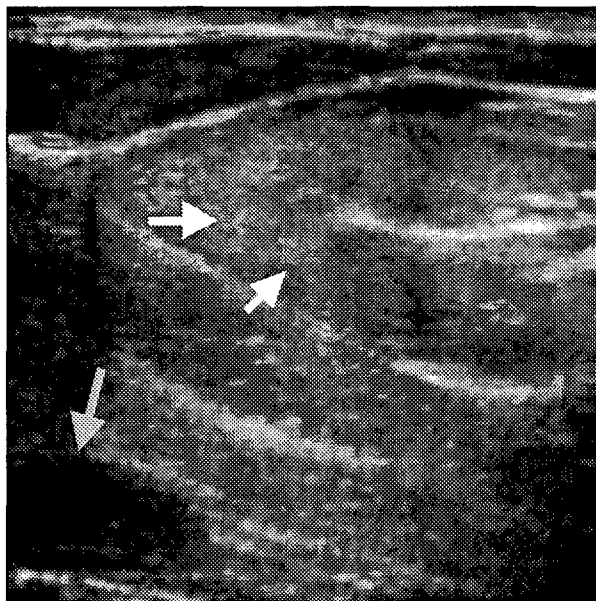
(d) Same image plane as (c) but from the same compounded image set as (b). Again note the slightly hypoechoic, lobulated inhomogeneities surrounding the left end of the hyperechoic structure on the central right (e.g., white arrows), corresponding to those at the white arrow in (b). Note also the improved delineation of the dark muscle or rib in the lower left (gray arrow) and the tissue striations extending to the right of it.

5
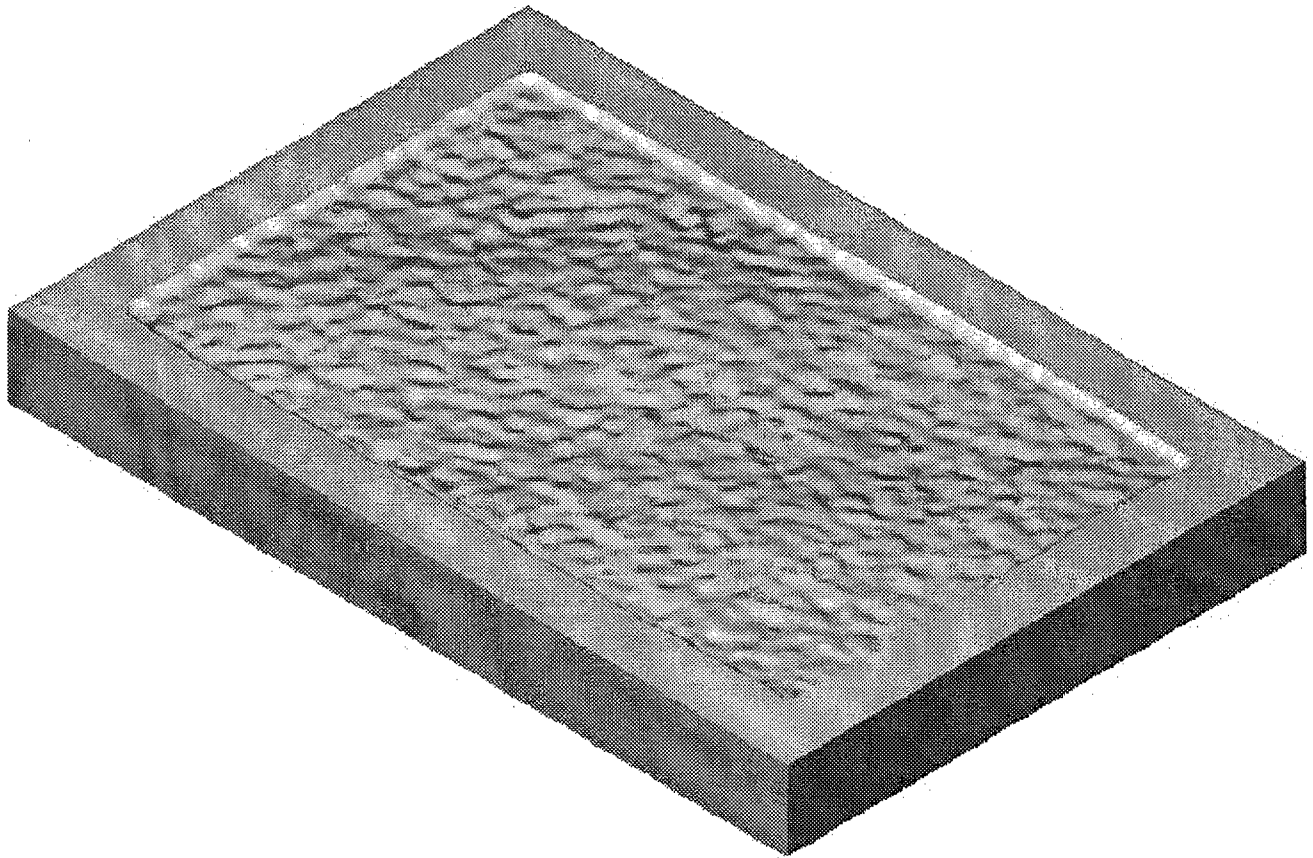
Figure 3. CNC design for the mold of an aberration plate introducing phase and steering errors similar to those found in breast tissue. The aberrator will be 60 by 100mm, and consist of 950m/s silicone rubber, filled with 1540m/s material. The undulations are about ±1.1mm deep (peak-peak) and include beam steering errors as well as defocusing.
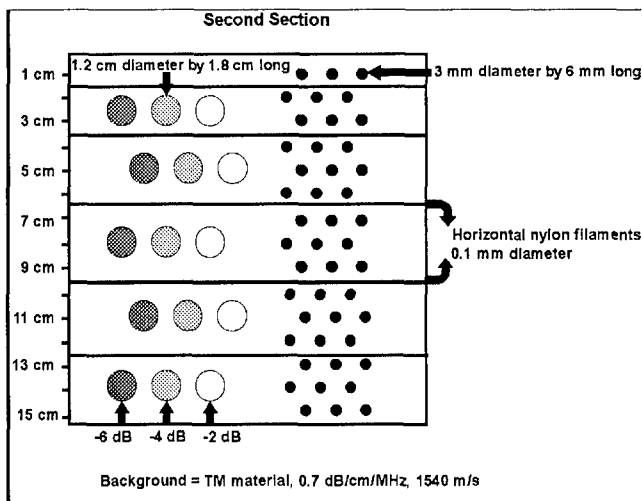
Figure 4. Diagram of our existing CIRS Model 44 cylindrical plug phantom, which we developed jointly with CIRS. Within the 5.5 cm range useable for the GE M12 scanhead, the front side shown contains 15 3 x 6 mm cylindrical plugs and the back side of the phantom, parallel to this side, contains 15, 1.5 mm x 2.4 mm long, and 15, 3 mm x 3 mm, cylindrical plugs of high contrast, ~-12 dB re the background material. This yields a total of 45 plugs with easily localized centers. Specific attenuation of the background material on the back side is 0.5 dB cm^{-1} MHz^{-1}. With and without the surface aberration plate of Fig. 3-4.6, this phantom will provide excellent measures of the change in resolution (contrast of the small plugs) and increase of contrast to noise ratio on the large, low contrast cylinders.

6

V. CONCLUSIONS

Considerable innovative work to improve and evaluate ultrasound imaging of breast cancer has been accomplished with primary or secondary support from this contract. Several of these advances are receiving national attention (References 6 & 8).

Clinical Trials

The 3D color flow quantification and other advances described above should increase the sensitivity and specificity of ultrasound imaging for discrimination of benign and malignant masses. They should also improve tracking of changes during treatment or even detection of masses by highlighting of subtle changes in follow-up studies. Data analysis and write-up of earlier trials has been completed and contributions were made to advance 3D image acquisition, display and quantification.

Compound and Sequential Imaging

The registration achieved so far is not at pixel level yet to allow accurate pixel-by-pixel correlation of velocity and power information in the calculation of v•NPD, but the registration is much better than can be done with visual identification of corresponding regions of interest and more complete delineation of gray scale and flow structures is provided. Fig. 2 reveals the success of techniques required to: 1) use the 3D registration for combining information from several types of ultrasound scans to provide an image volume of improved information content; 2) for following changes in the patient in serial exams. Both, but particularly the latter, can revolutionize medical imaging and interpretation. The former is approaching the quality necessary to allow compound scanning (imaging the same tissues from different viewing angles) in at least some cases and combining dedicated high resolution, (multifocal) gray scale images with f-CDI and/or p-CDI scans. These combinations will reduce speckle and electronic noise, while revealing more of the structure seen only at a few of the image look directions. The combinations also will allow time for higher resolution imaging in each mode while combining the different information from each. The types of serial exams that might be followed include tracking of tumor size and vascularity for early indications of response to treatment, as well as serial follow-up or even screening exams to reveal abnormal growth .

Image-based Slice Positioning [IBaR]

The possibility of practical implementation has been demonstrated commercially, albeit in a reduced form from what we have published (References 7 and 9). We believe it will be practical to make high quality 3D scans, that are either linear or sector, but possibly not both. The ability to make accurate distance measurements will probably be limited to fairly short distances and to areas around relatively uniform tissues.

Digital ductography development

The functional part of the breast is the glandular tissue which is found in 15-20 lobes which radiate out from the nipple. Each lobe is drained by its central duct which exits from the nipple. Almost all breast cancer occurs in the glandular tissue, and a significant proportion is intraductal. Therefore, being able to find and map the ducts might greatly increase the efficacy of B mode ultrasound for breast cancer screening and diagnosis. Display of the ductal tree in 3D, while panning through the gray scale images should be a significant aid to orientation and anatomy. At the least it will facilitate registration of serial volume image sets of the breast.

VI. REFERENCES

1. * LeCarpentier, G.L., Tridandapani, P.B., Fowlkes, J. B., Roubidoux, M. A., Moskalik, A.P. and Carson, P. L. Utility of 3D ultrasound in the discrimination and detection of breast cancer, RSNA EJ, 1999, http://ej.rsna.org/ej3/0103-99.fin/titlepage.html .

2. * Meyer CR, Boes JL, Kim B, Bland PH, LeCarpentier GL, Fowlkes JB, Roubidoux MA, Carson PL, Semiautomatic Registration of Volumetric Ultrasound Scans, Ultrasound Med. Biol., 25/3, 339-347, 1999.

3. ** Krüker JF, LeCarpentier GL, Meyer CR, Fowlkes JB, Roubidoux MA, Carson PL, 3D Image Registration for Multimode, Extended Field of View, and Sequential Ultrasound Imaging, RSNA EJ, http://ej.rsna.org/ej3/0098-99.fin/index.html .

4. ** Krücker JF, Meyer CR, Tuthill TA, LeCarpentier GL, Fowlkes JB, Carson PL. 3D compounding of B-scan ultrasound images. Joint Meeting: 137th Meeting of the Acoustical Society of America and 2nd Convention of the European Acoustics Association, Berlin, 15-19 March, 1999, Collected Papers (CD), ISBN 3-9804568-5-4, # 4ABB_3, 1999, 4pp.

5. ** LeCarpentier, G. L., Bhatti, P.T., Roubidoux, M.A., Fowlkes, J.B., Helvie, M.A., Carson, P.L. (1999b). Characterization of benign versus malignant breast lesions using frequency shift color Doppler imaging in conjunction with gray scale features and patient age. Visualizing the Future of Biology and Medicine, Bethesda, MD, NIH, http://www.capconcorp.com/grants/becon/meeting99/poster.htm.

6. ** Carson PL (primary author), (1999) Technological needs for improvement of ultrasound in detection of preclinical breast disease in high risk women. Draft report for Working Group on Novel Breast Ultrasound Technology, Amer. Col. Radiol., 3 pp. Not included, still confidential, no copyright release.

7. ** Tuthill TA, Krücker JF, Fowlkes JB, Carson PL (1998) Automated 3-D US Frame Positioning Computed from Elevational Speckle Decorrelation, Radiology, 209, 575-582.

8. Merritt, C. R. (1999). "Future directions in breast ultrasonography." Sem. in Breast Disease 2: 89-96.

9. Chen J-F, Fowlkes JB, Carson PL, Rubin JM: Determination of Scan-Plane Motion Using Speckle Decorrelation. Theoretical Consideration and Initial Test, Internat. J. Imaging Systems and Technology, 8, 38-44, 1997.

VII. APPENDICES

* = supported primarily by another grant

** = supported primarily or equally by this contract

1. * LeCarpentier, G.L., Tridandapani, P.B., Fowlkes, J. B., Roubidoux, M. A., Moskalik, A.P. and Carson, P. L. Utility of 3D ultrasound in the discrimination and detection of breast cancer, RSNA EJ, 1999, http://ej.rsna.org/ej3/0103-99.fin/titlepage.html .

2. * Meyer CR, Boes JL, Kim B, Bland PH, LeCarpentier GL, Fowlkes JB, Roubidoux MA, Carson PL, Semiautomatic Registration of Volumetric Ultrasound Scans, Ultrasound Med. Biol., 25/3, 339-347, 1999.

3. ** Krüker JF, LeCarpentier GL, Meyer CR, Fowlkes JB, Roubidoux MA, Carson PL, 3D Image Registration for Multimode, Extended Field of View, and Sequential Ultrasound Imaging, RSNA EJ, http://ej.rsna.org/ej3/0098-99.fin/index.html .

4. ** Krücker JF, Meyer CR, Tuthill TA, LeCarpentier GL, Fowlkes JB, Carson PL. 3D compounding of B-scan ultrasound images. Joint Meeting: 137th Meeting of the Acoustical Society of America and 2nd Convention of the European Acoustics Association, Berlin, 15-19 March, 1999, Collected Papers (CD), ISBN 3-9804568-5-4, # 4ABB_3, 1999, 4pp.

5. ** LeCarpentier, G. L., Bhatti, P.T., Roubidoux, M.A., Fowlkes, J.B., Helvie, M.A., Carson, P.L. (1999b). Characterization of benign versus malignant breast lesions using frequency shift color Doppler imaging in conjunction with gray scale features and patient age. Visualizing the Future of Biology and Medicine, Bethesda, MD, NIH, http://www.capconcorp.com/grants/becon/meeting99/poster.htm, Poster only.

Back to Contents   Send Letter   Appendix 1

Utility of Three-dimensional US in the Discrimination and Detection of Breast Cancer

Gerald L. LeCarpentier, PhD, Pamela T. Bhatti, MS, J. Brian Fowlkes, PhD,
Marilyn A. Roubidoux, MD, Aaron P. Moskalik, MS, Paul L. Carson, PhD

Department of Radiology
University of Michigan Medical Center
Ann Arbor, Mich, USA

Correspondence:
Gerald L. LeCarpentier, PhD
Department of Radiology
University of Michigan Medical Center
Kresge III Room 3315
200 Zina Pitcher Place
Ann Arbor, MI 48109-0553
Voice: (734) 647-9326
Fax: (734) 764-8541

Table of Contents

- Abstract
- Introduction
- Data Acquisition and Processing
    - o Image Acquisition
    - o Scanning Apparatus
    - o Post-Acquisition
    - o Regions of Interest
- Examples of Volume Rendering
    - o 3D Rendering of Infiltrating Ductal Carcinoma
    - o Various 2D Reconstructions
- Clinical Discrimination Results
    - o Speed-weighted Pixel Density
    - o Comparison With Gray Scale
- Discussion and Conclusions

Utility of Three-dimensional US in the Discrimination and Detection of Breast Cancer

Gerald L. LeCarpentier, Pamela T. Bhatti, J. Brian Fowlkes, Marilyn A. Roubidoux, Aaron P. Moskalik, Paul L. Carson

Abstract

The purpose of this article is to demonstrate evaluation techniques for three-dimensional (3D) ultrasound (US) imaging and their potential application in the discrimination and assessment of breast cancer. Our ongoing studies include women with mammographically observed breast masses scheduled for biopsy. During US imaging of suspicious breast lesions, transducer position is encoded for each power-mode and frequency-shift color Doppler image and for each standard B-mode image, typically 90 images in each mode. Vessels are then displayed as reconstructed color volumes in 3D, superimposed on gray-scale sections. Radiologists identify suspicious masses and rate their appearance for conventional gray-scale assessment and for the new vascular criteria. In an initial patient population, US discrimination of malignant masses in 3D volumes demonstrated superiority over their two-dimensional counterparts. In the related patient group presented here, one particular vascularity measure, speed-weighted pixel density, showed statistically different ($P < .001$) values for benign ($n = 13$) versus malignant ($n = 15$) cases. Given the authors' modest success in discriminating breast cancer in an initial patient pool with use of other vascularity measures, results of this second patient population continue to suggest vascularity as a potential cancer discriminator.

Utility of 3D US in the Discrimination
and Detection of Breast Cancer

Introduction

Subjective assessment of Doppler ultrasound (US) imaging may be enhanced by more-quantitative analyses. Displaying vascularity in three dimensions is relatively simple, since the image segmentation is performed by the color Doppler flow imaging system, and sparse vascular patterns are easily appreciated in three dimensions. A number of investigators (1-4) have done a good job of semiquantitative evaluation of color Doppler flow image characteristics of the breast; however, it may be difficult to objectively sample the sparse breast vasculature throughout the tumor volume in totally free-hand two-dimensional (2D) sampling. Stavros et al have achieved promising results in the evaluation of breast cancer by using a multivariable gray-scale assessment of 2D imaging (5,6). Cosgrove and Lees also indicated that the addition of color Doppler flow imaging to B-mode imaging improved the diagnostic accuracy by an amount approximately equal to the benefit of adding US to mammography. They state that the chance of malignancy after workup must be less than 2% to consistently avoid biopsy (7).

Based on the potential benefits of combining three-dimensional (3D) sampling and quantitative assessments, a preliminary study was performed to evaluate which Doppler signals might provide discrimination of breast cancer from benign masses and to compare 2D and 3D US display modes. The amount of blood flowing as indicated by power-mode color Doppler imaging (p-CDI) (8) and the velocity indicated by mean-frequency color Doppler imaging (f-CDI) both lend themselves to quantitative measurement (9). To evaluate information provided with these measurements and to aid in visual assessment, we undertook a visual and digital analysis of information in a study that included 3D US studies of 20 breast patients scheduled for breast biopsy. We have subsequently analyzed studies of 28 patients, obtained with a different scanner. Three-dimensional breast lesion image volume acquisition techniques and visualization schemes are presented here in general, and a particular vascularity measurement (speed-weighted pixel density) obtained in each of four regions of interest (ROIs) in and around the mass is compared with standard gray-scale criteria for this current patient pool.

Utility of 3D US in the Discrimination
and Detection of Breast Cancer

Examples of Volume Rendering

Figures 2 and **3** are taken from our second, and current, patient population. They serve to demonstate how lesion boundaries can be defined for subsequent quantitative calculations, as well as provide an appreciation of the 3D gray-scale and and vascular renderings. A revealing example of the information available with dynamic 3D can be seen in **Figure 3**. In our chosen coordinate scheme, x represents the lateral direction, y the axial direction, and z the elevational direction. Thus, the scan plane itself can be considered a constant "z" plane, having x-y (lateral-axial) coordinates. Similarly, the plane perpendicular to both the scan plane and the skin surface is considered the constant "x" plane, while the plane at constant depth (C-scan) is the "y" plane. Note in **Figure 3a** and **3b** the excellent section-thickness (elevational) resolution obtained with this matrix array (so-called 1.5 D) transducer.

a.

b.

c.

d.
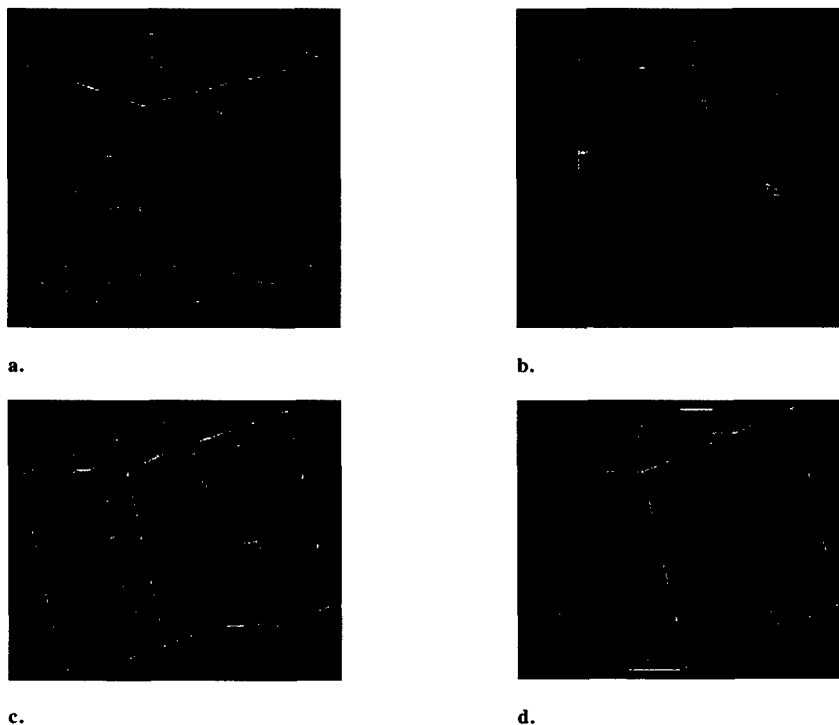
Figure 2. Two-dimensional and 3D power mode display of an elongated infiltrating ductal carcinoma in an 81-year-old woman. **(a)** Three-dimensional view demonstrates two planes, one of which is the original scan plane and the second an orthogonal plane that depicts the extent of the hypoechoic mass. **(b)** Two-dimensional image of the original scan plane demonstrates a vessel penetrating the mass. **(c)** Three-dimensional image with an ellipsoidal ROI defined by the gray-scale borders of the mass, for quantification of vascularity. The ROI is shown as a translucent green ellipsoid, to depict the approximate extent of the lesion, with the penetrating vessel seen as red. **(d)** Three-dimensional display with ROI in green and surface rendering of the vascularity in blue. *(Click any image to view its full-size version [<100 kB each])* .

a.   b.   c.

d.   e.   f.
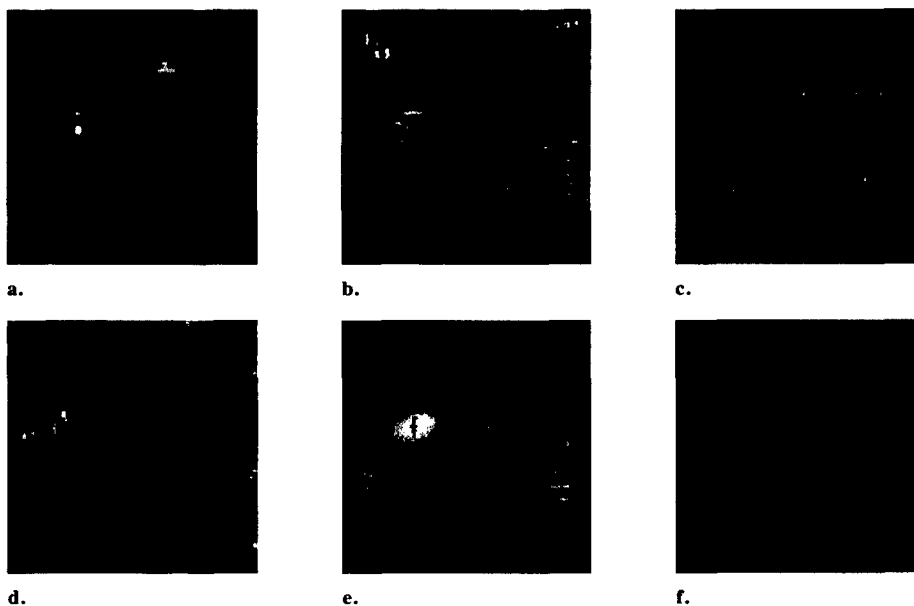
Figure 3. US scans of a 58-year-old woman with a nonpalpable mammographic lesion suspicious for cancer. On the clinical mammogram, the suspect region appeared as a 1.3-cm macrolobular circumscribed mass with no microcalcifications. Final pathologic studies revealed carcinosarcoma (half ductal, half chondrosarcoma). **(a)** Lateral-axial plane (scan plane, or z plane). The smooth ellipsoidal borders (approximately 1.6 x 0.9 cm) of the mass, approximately 0.6 cm from the surface, could cause the reviewer to miss the clearly malignant features in other views. **(b)** Axial-elevational plane (transverse plane, or x plane). The shadowing in this view suggests malignancy, particularly on the right side of the overall mass shown. **(c)** The plane shown here is arbitrarily oriented off either of the axes of the scan plane or transverse plane, and is slightly tilted. The slight outcropping and shadowing on the right side of the mass further suggests a malignant portion to this overall hypoechoic region. **(d)** Lateral-elevational plane (C-scan plane, or y plane). In this constant-depth view, unavailable from the scanner itself, note the malignant multilobular diffuse appearance of the mass. **(e)** The tumor shows ROI definition in 3D and 2D views. **(f)** Three-dimensional view shows irregular margins. *(Click on images* **a-d** *to view full-size versions; images* **e** *and* **f** *link to Quicktime movies [<1 MB each])* .

<p style="text-align:center">Utility of 3D US in the Discrimination
and Detection of Breast Cancer</p>

Clinical Trials and Vascularity Measures

Analysis of Clinical Results

Measures of the amount of blood in a region (NPD_{max}) and estimate of perfusion ($[V_m][NPD_{max}]$), mathematically defined in Table 1 (where *max* refers to the the maximum value calculated in the four regions described in Table 2), were plotted versus average gray-scale rating (1 = normal to 5 = highly suspicious) and were evaluated for each subject in the previous study (10). Using discriminant analysis to classify cancer versus benign masses and insisting on sensitivities of 100%, we achieved specificities of 82% and 90% for NPD_{max} and ($[V_m][NPD_{max}]$), respectively, when combined with gray-scale ratings. These specificities were higher than for gray scale alone, but the statistical uncertainty in these numbers is large. Our second patient pool is aimed at adding greater statistical significance to these values and exploring other possible quantitative measures. **Figure 4** demonstrates one such measure, speed-weighted pixel density (SWD), as described in Table 1. It is mathematically equivalent to pixel density times the average velocity and is thus similar to ($[V_m][NPD_{max}]$) without the power weighting. SWD_{max} refers to the the maximum or peak SWD value calculated in the four regions described in Table 2. As shown in **Figure 4**, the mean value of $\log(SWD_{max})$ is significantly different for the benign versus malignant groupings ($P < .001$ that the mean values are equal).
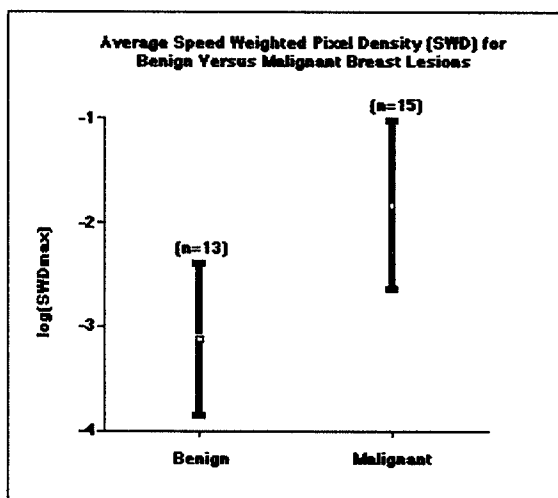
Figure 4. Plot of the $\log(SWD_{max})$ (ie, the maximum SWD value for the four ROIs described in **Table 2**) for benign versus malignant breast lesions. Mean values and their standard deviations are shown for the two poopulations. As demonstrated by t test results, the probability that the mean values of these subgroups are different was statistically significant ($P < .001$).

Comparative Results

Receiver operating characteristic (ROC) analysis was performed on the SWD measure and average gray-scale rating using ROCKIT software provided by the University of Chicago's Department of Radiology (from the current version of an ROC software package developed by Charles E. Metz, PhD, and his colleagues). **Figure 5** demonstrates the predictive similarity between the SWD measure and the average gray-scale rating. The graph shows the raw data and maximum likelihood estimates of single binormal ROC curves for both measures, given a subject pool of 28 patients. The Az values calculated for SWD and gray scale were comparable, 0.88 and 0.84, respectively.
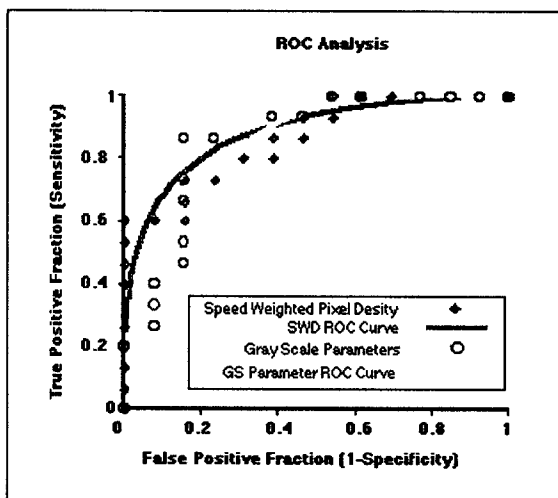
Figure 5. Calculated true-positive fractions versus false-positive fractions of $\log(SWD_{max})$ and average gray-scale ratings for our 28-patient population. Overlaid are smooth calculated ROC curve estimates. Although the area under the curve was slightly greater for SWD performance, the difference in the two areas (Az[SWD] = 0.88 versus Az[GS] = 0.84) was not significant. *GS* = gray scale.

Utility of 3D US in the Discrimination
and Detection of Breast Cancer

Discussion

Our data transfer, processing, and visualization tools have been developed to the point where full 3D volumes and vascularity surface renderings can be reviewed within an hour of the US examination itself. These developments have facilitated the visualization of vascular morphology and made easier scanning through entire US volume sets from different perspectives. In addition, we have provided the radiologist with a straightforward method for defining reproducible ROI ellipsoids within a given US volume, which facilitates a variety of quantitative measures. As demonstrated by means of ROC analyses, these objective measures of vascularity (most recently SWD) in and of themselves have been shown to be as effective as subjective gray-scale measures for our current patient population.

Given these observations, we believe that vascularity measures should improve the discrimination of benign and malignant solid masses with US and that the results are probably applicable to different scanners. Larger numbers of subjects and improved ease of performance of good vascularity examinations are now needed to allow good judgments of the achievable diagnostic accuracy and cost-effectiveness of adding vascularity to clinical US assessments of breast masses.

Ease of performance is well on its way, with advances occurring rapidly in 3D scanning, image analysis, and image display. If power-mode and color Doppler flow measures (NPD and SWD) each, separately, continue to perform comparably with gray-scale measures and almost as well as the power-mode and color Doppler flow combination required for $\log[(V_m)(NPD_{max})]$ as demonstrated in our earlier report (9), then one of the two color Doppler flow 3D scans can be eliminated to speed up the entire process. Alternatively, the US system manufacturer could supply the power frequency signals simultaneously with sufficient signal dynamic range for accurate assessments of the perfusionlike $\log[(V_m)(NPD_{max})]$ on a pixel-by-pixel basis. For imaging vessel patterns, little would be lost by requiring the same system settings for both frequency-shift and power modes in a single image.

In these studies, gray-scale readings were performed by a radiologist highly experienced in breast imaging and US. If vascularity measures on simple ROIs can perform at least as well as gray-scale assessments for the experienced reader, the potential for use of vascularity measures in improving routine diagnosis is high.

Conclusions

Our modest success in discriminating breast cancer in an initial patient pool with other vascularity measures and the results from this second patient population continue to suggest vascularity as a potential cancer discriminator. Our visualization and quantization tools should continue to facilitate this process.

Utility of 3D US in the Discrimination
and Detection of Breast Cancer

References

1. Carson PL, Adler DD, Fowlkes JB, Harnist K, Rubin J. Enhanced color flow imaging of breast cancer vasculature: continuous wave Doppler and 3-D display. J Ultrasound Med 1992; 11:377-385.

2. Bamber J, Eckersley R, Cosgrove D, Bell D, Kedar RP. 3-D reconstruction of combined colour Doppler and grey scale images of breast tumours. In: Madjar H, Teubner J, eds. Breast ultrasound update. Basel, Switzerland: Karger, 1993.

3. Cosgrove DO, Kedar RP, Bamber JC, et al. Breast diseases: color Doppler US in differential diagnosis. Radiology 1993; 189:99-104.

4. Cosgrove DO, Bamber JC, Davey JB, McKinna JA, Sinnett HD. Color Doppler signals from breast tumors: work in progress. Radiology 1990; 176:175-180.

5. Stavros AT, Parker SH, Dennis MA, Johnson KK, Thickman DI, Rapp CL. Sonography of solid breast nodules: benign or malignant? (abstr). Radiology 1993; 189(P):406.

6. Stavros AT, Thickman D, Rapp CL, Dennis MA, Parker SH, Sisney GA. Solid breast nodules: use of sonography to distinguish between benign and malignant lesions. Radiology 1995; 196:123-134.

7. Cosgrove DO, Lees WR. Abdominal ultrasound workshop. Eurodop, European Doppler Ultrasound Symposium, Oxford, England, 1994.

8. Rubin JM, Adler RA, Fowlkes JB, et al. Fractional moving blood volume: estimation with power Doppler US. Radiology 1995; 197:183-190.

9. Carson PL, Fowlkes JB, Roubidoux MA, et al. 3D color Doppler image signal quantification of breast masses. Ultrasound Med Biol 1998; 24:945-952.

10. Carson PL, Li X, Pallister J, Moskalik AP, Rubin JM, Fowlkes JB. Approximate quantification of detected fractional blood volume and perfusion from 3D color flow and Doppler power signal imaging. In: Ultrasonics Symposium proceedings. Piscataway, NJ: IEEE, 1993; 1023-1026.

11. Carson PL, Moskalik AP, Govil A, et al. The 3D and 2D color flow display of breast masses. Ultrasound Med Biol 1997; 23:837-849.

12. Fenn RC, Fowlkes JB, Moskalik AP, Zhang Y, Roubidoux MA, Carson PL. A hand-controlled, 3-D ultrasound guide and measurement system. Acoustical Imaging, 1997; 22:237-242.

PII S0301-5629(98)00148-3

● *Original Contribution*

SEMIAUTOMATIC REGISTRATION OF VOLUMETRIC ULTRASOUND SCANS

CHARLES R. MEYER, JENNIFER L. BOES, BOKLYE KIM, PEYTON H. BLAND,
GERALD L. LECARPENTIER, J. BRIAN FOWLKES, MARILYN A. ROUBIDOUX, and
PAUL L. CARSON

Department of Radiology, University of Michigan Medical School, Ann Arbor, MI

Abstract —We demonstrate the ability to register easily and accurately volumetric ultrasound scans without significant data preprocessing or user intervention. Two volumetric ultrasound breast scan data sets were acquired from two different patients with breast cancer. Volumetric scan data were acquired by manually sweeping a linear array transducer mounted on a linear slider with a position encoder. The volumetric data set pairs consisted of color flow and/or power mode Doppler data sets acquired serially on the same patients. A previously described semiautomatic registration method based on maximizing mutual information was used to determine the transform between data sets. The results suggest that, even for the deformable breast, three-dimensional full affine transforms can be sufficient to obtain clinically useful registrations; warping may be necessary for increased registration accuracy. In conclusion, mutual information-based automatic registration as implemented on modern workstations is capable of yielding clinically useful registrations in times <35 min. © 1999 World Federation for Ultrasound in Medicine & Biology.

Key Words: Ultrasound, Mutual information, Registration, Volumetric, affine, Thin plate spline warping.

INTRODUCTION

There are potentially many reasons why ultrasound examinations might benefit from registration. Images from different transducer positions are at least partially, if not fully, uncorrelated, and summing them can significantly improve the contrast-to-speckle noise ratio. Doppler color flow acquisitions suffer from undetected flow where the flow is parallel to the transducer's face. Volumes collected from different viewing directions may detect such missing flow vectors, and registration across acquisitions can assist in computing flow velocity vectors that are consistent across different views. Perhaps the most important reason to register ultrasound data sets is to assist the comparison of serial examinations performed on the same patient. Presenting two-dimensional images from different serial examinations with the same orientation and partial volumes may help the clinician more easily to distinguish what has changed. To the extent that echogenicities from different examinations can be approximately equalized, registered serial examinations can be subtracted to emphasize changes. Such differential approaches could be especially important when serially monitoring patient response to chemotherapy or radiation therapy.

Although such automatic registration methods for ultrasound data sets may be desirable, there are preliminary reasons for caution in expecting automatic methods to function well. Such reasons include the ubiquitous speckle noise and attenuation artifacts such as "comet tails" of either shadowing or enhancement. Attenuation artifacts that present differently in each of the data sets depending on transducer orientation may compromise chances of successful registration for any automatic method. An additional source of inconsistent features comes from strong coherent echoes that are observed from structures large with respect to wavelength when observed in an orientation normal to the reflecting surface. Thus, coherent echoes as well as shadows in different data sets are often sources of inconsistent geometry when the data sets were acquired using different transducer orientations. Refraction, i.e., ray bending, may yield additional inconsistencies.

Address correspondence to: Charles R. Meyer, Department of Radiology, University of Michigan Medical School, Ann Arbor, MI 48109-0553, USA. E-mail: cmeyer@umich.edu
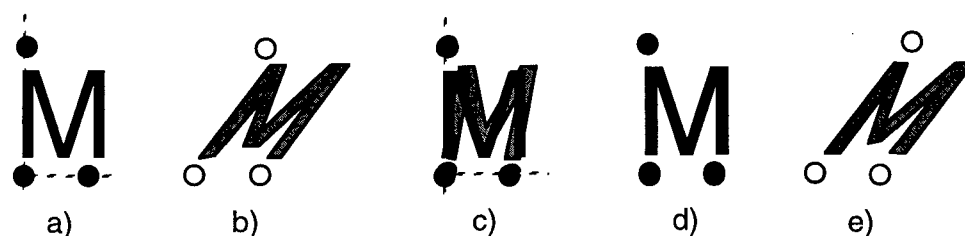
Fig. 1. A simplified two-dimensional example of the registration process is illustrated. (a, b) Two "multimodal" images in which the user has poorly chosen approximate homologous points. (c) Geometric registration that maps the corresponding markers onto each other after the user's initialization, but before automatic optimization begins. After initialization, although the markers are perfectly aligned, the images are still misregistered. (d) Resulting final registration obtained by the optimizer's driving the locations of the homologous points in (b) to minimize the cost function, $-I$, *i.e.*, maximizing I. (e) Note that the position of the upper marker in (b) has been moved by the optimization process to a new position. (Reproduced with permission from Oxford University Press from Medical Image Analysis 1997;3:195–206.)

The following paragraphs describe the use of a semiautomatic registration technique that appears to be capable of registering ultrasound data sets based on the preliminary information presented herein. The term "semi" qualifies the description of the otherwise totally automatic method because the initial pose between the two data sets must be set by the user. At present, the authors are unaware of any semi- or fully automatic registration algorithms that have been applied successfully to ultrasound data volumes. A recent review of registration techniques in general can be seen in Maintz and Viergever (1998).

METHODS

Volumetric ultrasound data were acquired using a 9-MHz linear array clamped to a linear slide and position encoder on a hand-held frame (Fenn et al. 1997). The transducer manually was swept across the tissue of interest in a direction normal to the linear array's scanning plane. Accuracy of beam position measurement relative to the scan frame was 0.1 mm in the focal plane of the transducer. Data volumes on a uniform Cartesian grid were created by trilinear interpolation between acquired images from known positions.

Pairs of such ultrasonic volumes were registered using a method that requires an initial rough guess of the orientation between the two data sets. As can be seen later in the Results section for the random void phantom, the initial orientation may be far from accurate, but will still within the capture range of the algorithm and result in an accurate registration. The initial, approximate orientation is computed by having the user position a minimum of three corresponding point pairs in each data volume. One of the data sets is chosen by the user as the reference data set, and the other data set, which will be geometrically transformed onto the reference, is referred

to as the homologous set. Points in both sets are deposited by clicking the computer's mouse as the cursor is positioned manually over similar-looking, three features. Then, under automatic control of the optimizer, the first three points in just the homologous data set are moved to recompute different geometric orientations of the homologous data set with respect to the reference data set. The points in the homologous data set are referred to as control points, because the geometric orientation between the two data sets is changed to satisfy the homology defined by the control points. The automatic optimizer repeatedly perturbs the loci of the control points in the homologous data set, such that the resulting mutual information, as computed for all voxels in the reference volume and all corresponding voxels in the homologous volume, is maximized to yield the final computed registration model between the two data sets (Collignon et al. 1995; Meyer et al. 1997; Studholme et al. 1997; Viola and Wells 1995; Wells et al. 1996). Figures 1, 2, and 3 help visualize the interplay among the control points, the computation of mutual information, and the recursive optimizer algorithm.

The entropy of a data set is defined as its average information content, whereas joint entropy is the average information of two ordered data sets. The joint entropy H(a,b) of two data sets, a and b, is related to mutual information of both, I(a,b), by the following classic relationship:

$$H(a,b) = H(a) + H(b) - I(a,b) \qquad (1)$$

where H(a) and H(b) are the individual entropies of data sets a and b, respectively (Papoulis 1984). As can be seen in the classic relationship, mutual information I(a,b) is the amount by which the sum of the individual data set entropies must be reduced to account for correlations that
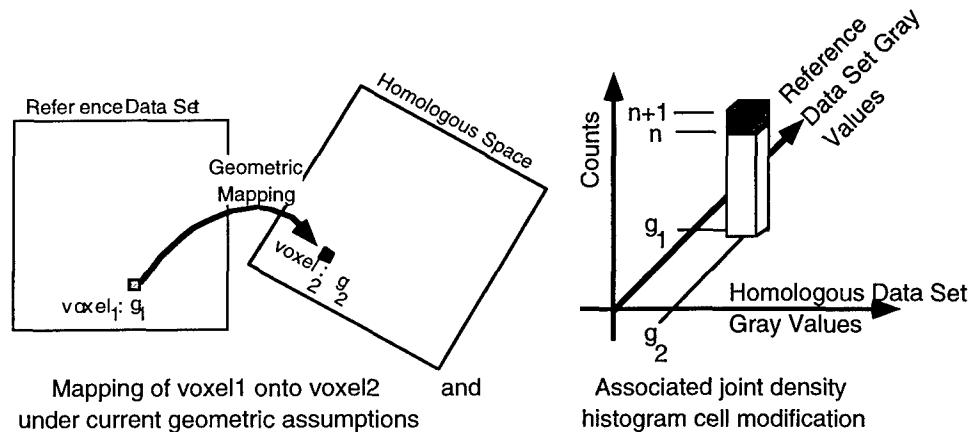
Fig. 2. Two-dimensional joint histogram constructed by raster scanning through all voxels in the reference image set and incrementing bin counts corresponding to the gray-scale values from geometrically mapped voxel pairs under an assumed geometric transformation, which changes with each iteration of the optimizer. (Reproduced with permission from Oxford University Press from Medical Image Analysis 1997;3:195–206.)

exist between the two individual data sets (H and I are non-negative). The previous expression defining mutual information in relation to entropies reduces to the following equation for mutual information in terms of the more fundamental probability density functions for data sets a and b:

$$I(a,b) = \int \int da\ db\ p(a,b)\ \log(p(a,b)/p(a)p(b)). \quad (2)$$

The initial geometric transform model optimized via moving the initial three control points is the simple, rotate–translate (six degrees of freedom) transform. In a subsequent optimization, the parameters for a full affine (linear, 12 degrees of freedom) transform are estimated via four control points (the three previous plus one new control point positioned automatically into the homologous data set using the previously optimized rotate–translate transform). Finally, if desired, repeated thin plate spline (TPS) warpings are computed using five or more control points as necessary, where the previous full affine optimum transform is used to instantiate the additional control points. In this manner, the mutual information is optimized at each stage of increasing geometric model complexity, while requiring the user only roughly to estimate approximate geometric homology for the three initial points. The additional control points beyond the first three, which eventually are mapped into the homologous data set, initially are placed in the reference
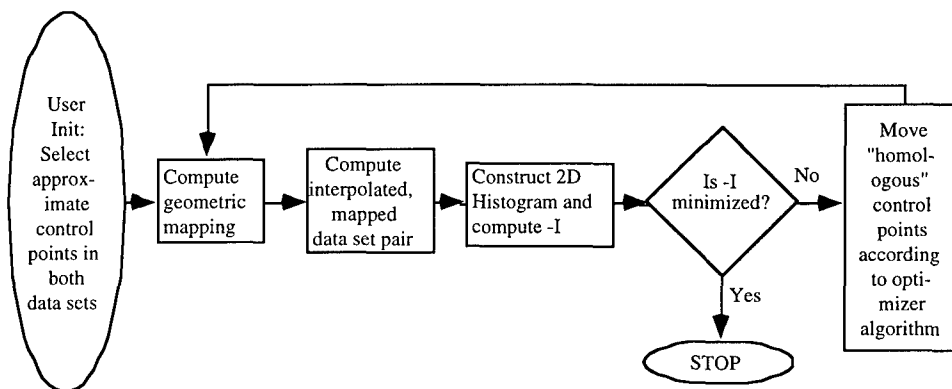
Fig. 3. Functional flow chart of the automatic registration algorithm for one optimization cycle. The process is repeated using the previously computed optimized control point positions as the new starting vector, until the incremental change in mutual information between cycles falls below a user set threshold, typically 0.0002 bits. (Reproduced with permission from Oxford University Press from Medical Image Analysis 1997;3:195–206.)
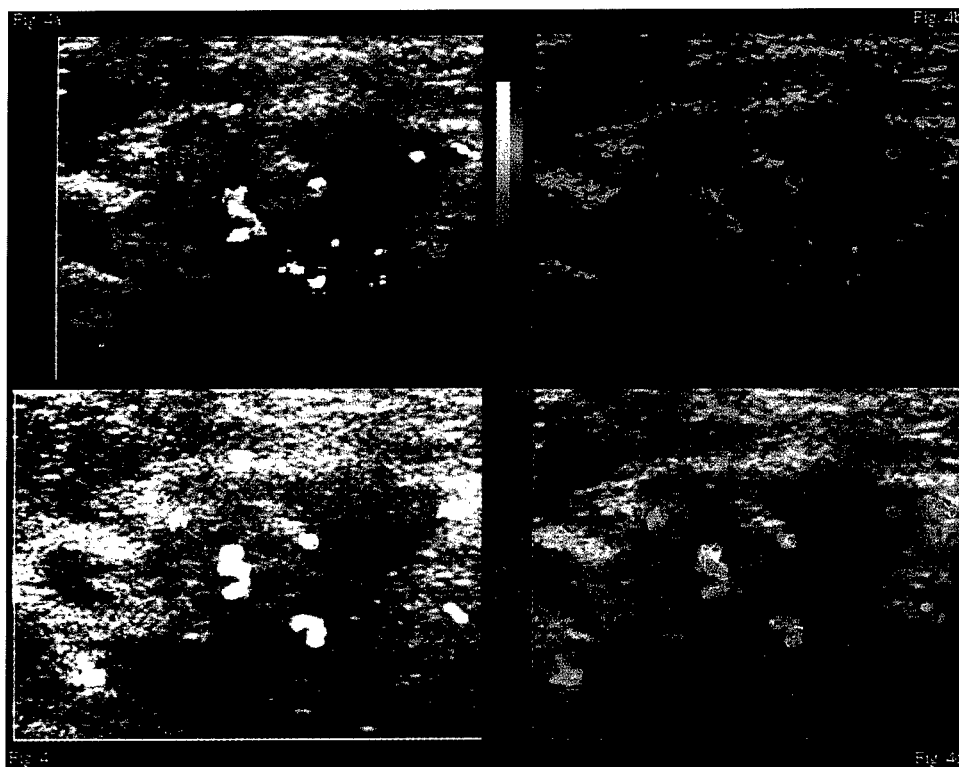
Fig. 4. (a) Image from the red channel of a color flow volume breast examination. (b) Pseudocolored image of (a). Lowest echogenicities are represented by dark blue, intermediate echogenicities by green, and highest echogenicities by bright red hues. Color mapping relationship is explicitly demonstrated in the attached gray-scale and color bars. (c) Power mode data corresponds to same loci as the color flow slice of a following registration. (d) Composite image constructed using "screen door" transparency, where adjacent pixels alternate between the color and gray-scale sources of (b) and (c).

data set by the user, without identification of corresponding positions in the homologous data set.

Uniformly sampled data volume sizes are approximately $400 \times 350 \times 55{-}100$ voxels depending on the manual acquisition; voxel volumes are typically $80 \times 80 \times 200$ μm^3. The registrations computed herein use decimated reference data sets to speed computation. During the initial use of the rotate-translate model, only every fourth voxel in the three major coordinate directions is used in the reference data sets. Each optimization cycle stops when the controller requests control point movements of less than some user chosen criterion, selected here as 0.1 mm, in each coordinate direction. The optimizer is the standard Nelder simplex algorithm, often referred to as "amoeba" (Press et al. 1988). Optimization cycles are repeated until the mutual information increment in the last cycle is less than or equal to another user chosen criterion, selected here and for almost all other modality pairings as 0.0002. After computing the optimal forward transform, which maps the homologous data set onto the reference, the high-resolution mapping of every voxel of the reference data set onto the homologous is computed once, using the inverse transform.

RESULTS

The first registered volumetric data set pair shown in Fig. 4 consists of color flow and power mode Doppler data sets acquired serially during the same patient examination visit. A three-dimensional, nine control point (27 degrees of freedom) thin plate spline warping was computed in 31 min of CPU time on a 200-MHz DEC Alpha workstation, model 3000/500x, using a total of 1552 iterations (where each iteration consists of calculating the geometric transformation, reconstruction of the mapped homologous gray-scale volume, joint histogram, and resulting mutual information) . The red channel of each data set pair was used to compute the geometric mapping. Although radiologists commonly avoid the use of pseudocolored images, such composite images assist in visualizing the results of registration. Display of the registered data sets as shown in Fig. 4d enhances visual differentiation of the individual image sources and facilitates the visual assessment of registration accuracy at all locations in a single image.

Figure 5 allows the reader to assess the accuracy of the volumetric registration over a large volume of sup-
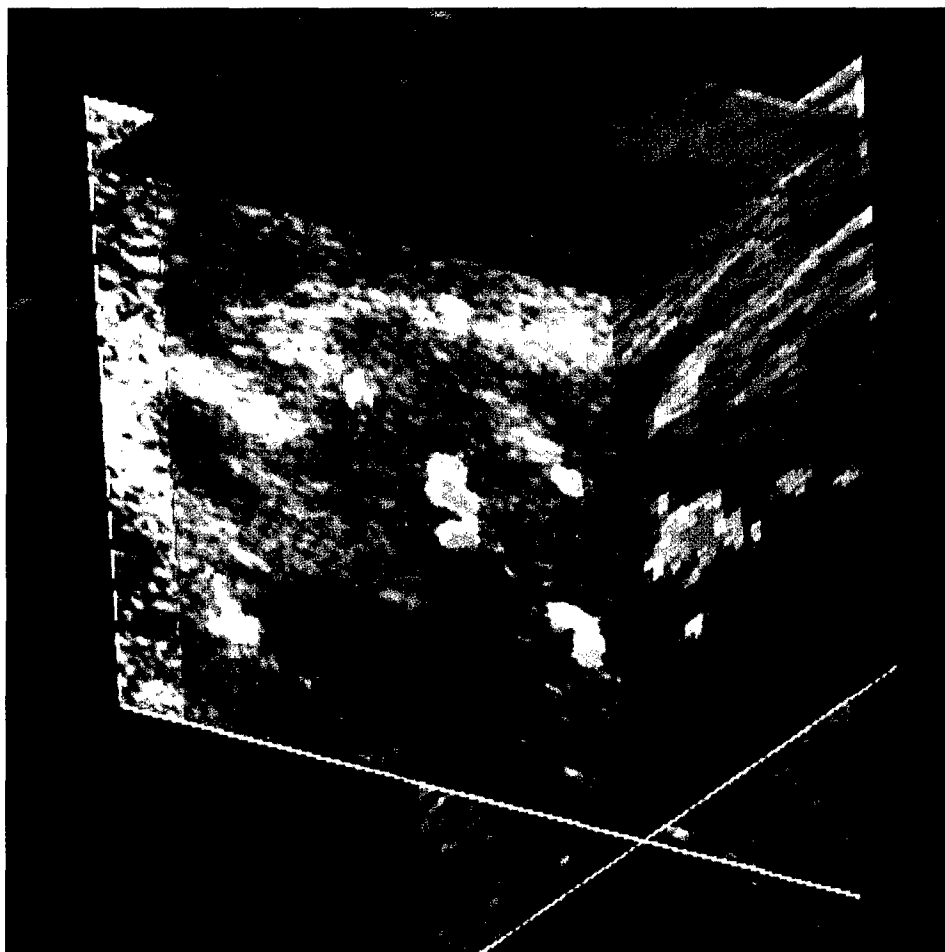
Fig. 5. View of the registered color flow and power mode volumes visualized on three orthogonal, intersecting cut planes using a color composite rendering method that approximates the screen door transparency shown in Fig. 4d. The observer's viewpoint presented here is one of looking back at the transducer from a distal position deep within the breast (top of the image is still patient's anterior). The cut plane whose orientation is nearly perpendicular to the viewer is the same image as that shown in Fig. 4d, where the underlying gray-scale image represents one of the (high resolution) acquisition planes of the color flow data volume. The intersecting cut plane across the top of the volume renders the registration at a constant, shallow depth below the transducer (C-mode), and the remaining cut plane right of center renders a slice of the registered volume below the line traversed by a single transducer element during the manual sweep of the transducer. The color bars that define the pseudocolor conversion for the reference scan is visible on the reader's left.

port. The color composite display computes the relative color contribution to each voxel, based on a linear combination of the intensities of the voxels of the two registered input volumes. The orthogonal cut plane method of display was chosen because of its clarity, intuition, freedom from confusing intervening structures, and the ability simultaneously to display spatially diverse, three-dimensional locations.

Figure 6a demonstrates the effects of the computed geometric warping, by applying the same warping to a rectilinear grid occupying the power mode volume. Figures 6b–6d show views of the deformation from the right, front, and top, respectively. Note that the major component of the geometric transform is a simple affine

transformation, as best seen in Fig. 6d, where the volume has been sheered to the left as a function of distance away from the observer, i.e., transducer position. Upon closer inspection, a nonlinear warp can be observed in the front central section of the volume, the same region occupied by the lesion, indicating that, during the second scan, the lesion moved differently than the surrounding tissue.

The second pair of registered volumetric data sets presented here consists of two power mode Doppler data sets acquired on the same patient and separated by 45 d during chemotherapy for locally advanced infiltrating ductal carcinoma. In contrast to the previous case, the registration model's complexity was capped at the level of the full affine (linear, 12 degrees of freedom) trans-
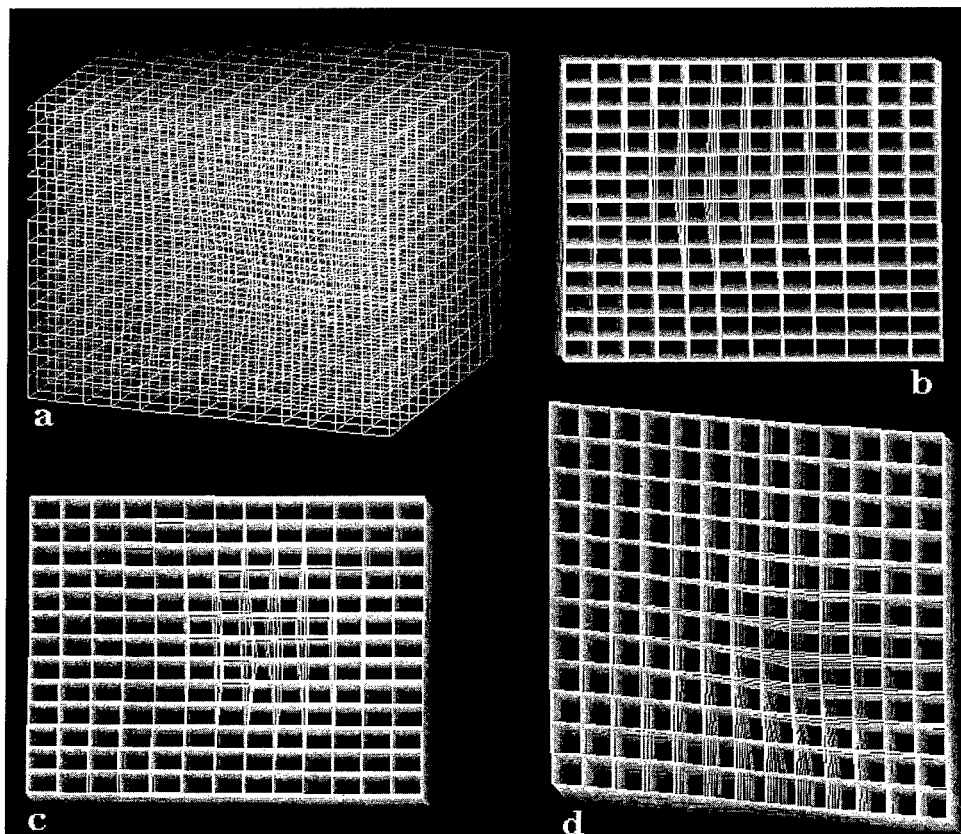
Fig. 6. (a) Computed geometric warp of the power mode volume is demonstrated by applying the same warp to a rectilinear grid occupying the initially undistorted power mode volume. (b, c, d) Views of the warped deformation from the right, front, and top of the scanned volume, respectively.

form due to the resulting excellent overall accuracy, as determined visually. Computing this transform from the initial rough estimate required 909 total iterations over the period of 11.3 min. As in the previous case, the red channel of each pair was used for computing the geometric mapping and display of results. Figure 7a shows three orthogonal cut planes through the registered data set volumes, as visualized from a position above the transducer looking deeper into the scanned volume. Note the shear (most appreciated on the plane nearly perpendicular to the viewer) required to register the data sets. Figure 7b is a single slice of the more recent data set, and Fig. 7c shows the data from the earlier scan corresponding to the geometry of the slice shown in Fig. 7b obtained after volumetric registration. Because the two cases were performed with nearly equivalent depth-gain compensation, equalization of the echogenicities of both scans was trivially achieved using linear gray-scale contrast adjustment. Figure 7d demonstrates the signed difference between the two scans, where the yellow hue represents differences of positive sign, the blue hue represents differences of negative sign, and the intensity for each hue is proportional to the magnitude of the difference. Al-

though some bright, horizontal, linear, coherent structures clearly are represented in the difference image, a lower contrast echogenic structure also is visualized (arrow), i.e., present in the earlier data set but missing in the later volume.

In addition to the two breast data sets presented herein, we include results from scanning a commercially available, random void phantom in two different orientations. The phantom is made by Computerized Imaging Reference Systems, Inc. (Norfolk, VA, USA) and consists of two slabs of randomly placed spherical voids surrounded by a random scattering medium having an attenuation of 0.5 dB cm^{-1} MHz^{-1}. One slab consists of 5-mm diameter voids, and the other consists of 3-mm diameter voids. The two slabs are separated by a voidless slab consisting of the same random scattering medium used to surround the voids in the other slabs. Scattering from the voids averages 14 dB down from the surrounding random scattering medium. Nylon fibers run parallel to the slabs at depth ranges of 2 and 6 cm.

One volumetric scan acquisition was made by manually translating the transducer parallel to the sides of the phantom and, thus, parallel to the wall of spherical voids
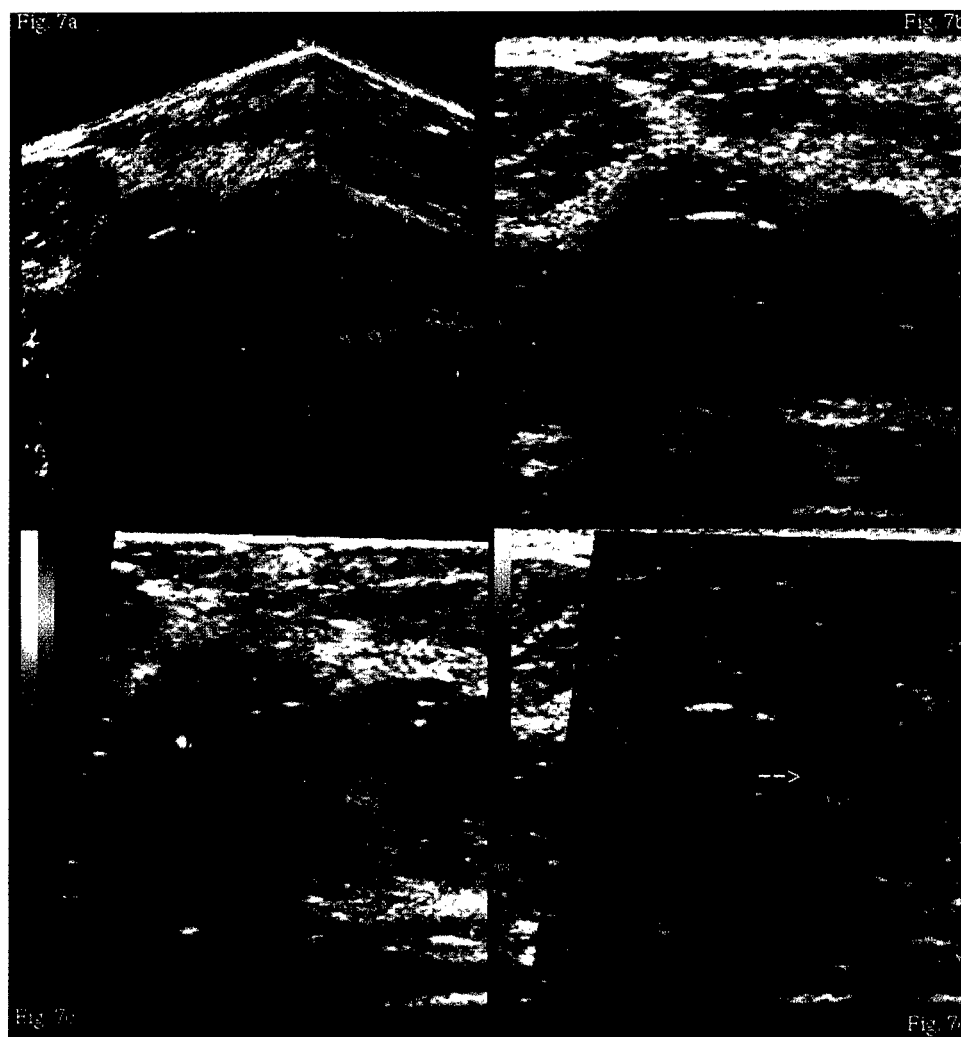
Fig. 7. (a) Orthogonal cut planes through the registered power mode data set volumes from serial examinations visualized from a position above the transducer looking deeper into the scanned volume. The pseudocolored volume was acquired 45 d earlier than the gray-scale volume. (b) Single slice of the more recently acquired data set. (c) Data from the earlier scan corresponding to the geometry of slice (b) after volumetric registration has been implemented; (c) also is visible as the pseudocolored component in (a). (d) Signed difference between (b) and (c), where the two hues represent differences of opposite sign, whereas intensity of each hue is proportional to the magnitude of the difference. In the color bar, a difference of +127 is represented by bright yellow, a difference of zero is black (center of bar), and a difference of −128 is bright blue.

with the transducer held approximately perpendicular to the phantom's surface. The second scan was taken by reorienting the translation path 45° to the initial position using a draftsman's triangle. Thus, in the second scan, the transducer remained approximately perpendicular to the phantom's surface, whereas the path of the translated transducer crossed the wall of voids diagonally. The initial poor placement of the starting markers was intentional, to demonstrate to the reader how severe misregistration of features appears (Fig. 8a) using the display technique shown in Figs. 4 and 5, where blended pseudocolor and gray-scale scans demonstrate the large capture

range of the automatic registration algorithm. Note that the bright gray-scale line in the homologous data volume represents the same nylon fiber in the phantom as the red pseudocolor line in the reference volume. The angular misregistration is readily apparent between the two data sets. Note that the voids appear to be filled with higher level scattering, due to the misregistration of the two data volumes.

The results of the final registration are presented in Fig. 8b. The linear nylon fiber in the homologous data set has been superimposed with the red pseudocolored reference data volume fiber. The linear fiber superimposi-
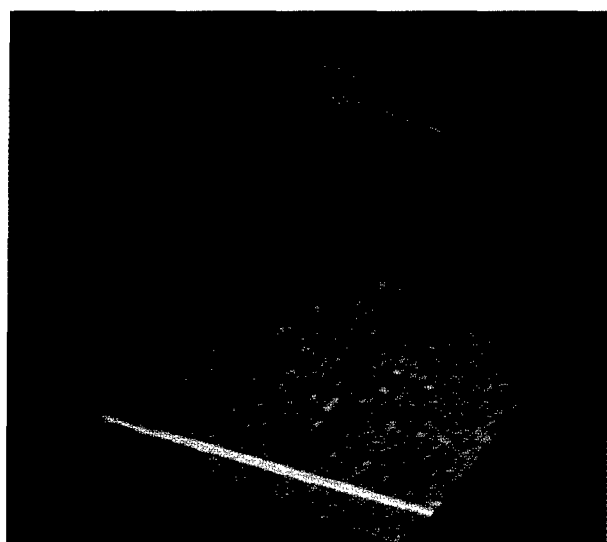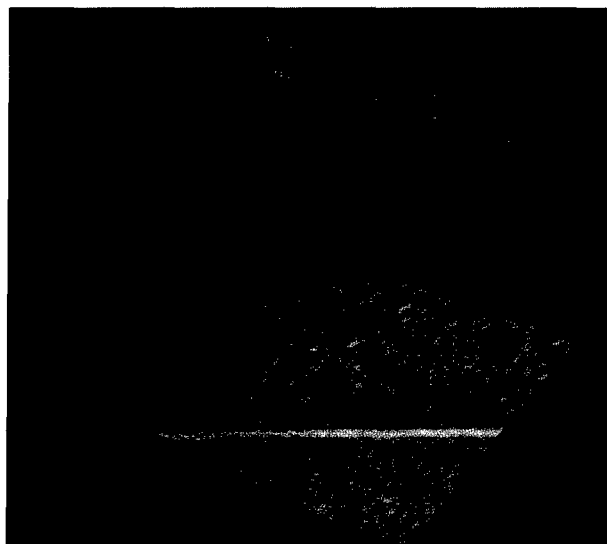
Fig. 8. (a) Initial pose of the 45° diagonal scan of void phantom in gray scale with 0° reference scan in pseudocolor is displayed on three orthogonal planes through data volume. Note the filled appearance of the voids as well as the lack of alignment of the linear nylon fiber in this initially misregistered pose. The reference data set is shown in pseudocolor, with the same color conversion relationship used previously. (b) The same display of reference data set shown in (a) after automatic registration of the volumetric 45° scan with the reference 0° scan. Note that, after registration, the voids have more contrast, because they are not inappropriately filled with misregistered scatterers, and the nylon fiber in the 45° scan is nearly collinear with its position in the reference volume.

tion is nearly perfect to the viewer's right, whereas a slight misregistration can be observed to the viewer's left, as a partial separation of both bright gray and red. This slightly visible error correlates well with the com-

puted angles of $-1.0°$, $-45.4°$, and $-0.5°$ for θ_x, θ_y, and θ_z, respectively, of the rotate-translate approximation to the computed full affine geometric transformation matrix; we would expect $0°$, $45.0°$, and $0°$ for a perfect result. The mutual information of the initial pose was 0.064 bits, which was optimized to 0.229 bits in 17 cycles of 1025 total iterations under the rotate-translate geometry model, and finished at 0.383 bits after 16 additional cycles consisting of a total of 1869 iterations, using the full affine geometry model. It is worth noting that simple low-pass filtering of the two data sets significantly speeds the convergence of the registration algorithm, by reducing the grand total of all iterations to 1200, which require total compute times <9 min on a 433-MHz DEC Personal Alpha workstation.

DISCUSSION

Volumetric registration was computed in all cases using a full affine transform as the first endpoint. If the resultant registration was judged by visual inspection to be flawed in local regions, a higher degree of freedom geometry model, i.e., warping, was computed. Thus, the thin plate spline warping of the data set associated with Figs. 1 and 2 was implemented using both a number, i.e., nine, and placement of control points that resulted in a better global solution. The improved accuracy of the registration resulting from warping was determined both visually and quantitatively by the increase in the final, optimized mutual information, i.e., a significant 27% increase in I was observed from 0.805 for the full affine solution to 0.827 for the nine point TPS solution. The presence of a small mass with different elastic modulus than the surrounding tissue is suggested by observing the nonlinear warping depicted in Fig. 3, because the computed tissue deformation indicates a local rotation. This rotation could have been in response to the overall deformation caused by the pressure of the transducer on the skin in the process of scanning.

For the case of the void phantom, although the error associated with θ_y was <0.5° from the expected value of 45°, the error of 1° in θ_x can be explained by our inability accurately to mount the transducer perpendicular to the plane of the manual translation baffle. Any deviation away from 90° in the angle subtended by the rotation of the autoscanning plane of the transducer into that of the manual scanning baffle, i.e., θ_x, will require compensation by both θ_x and θ_z, depending on the rotation imposed on θ_y. Additional registration accuracies using phantom data from computed tomography, magnetic resonance imaging, and positron emission tomography, are available in Meyer et al. (1997). Although no preprocessing was necessary for the phantom data to obtain accurate registrations, a >50% decrease in registration

time was obtained by low-pass filtering the input data sets before registration. Such behavior should be expected, because low-pass filtering increases the long range correlations in the data sets and smoothes the resulting cost function, such that convergence can be obtained without entrapment by many local maxima.

Because bright, linear structures in the scanned volume occur when the transmitted beam is perpendicular to an echogenic surface, a lack of overlapping alignment of such linear structures is expected, due to the variation in transducer angles used to acquire the different volumes. Conversely, good registration of less intense, incoherent backscattering structures is expected and should be used as an independent visual evaluation tool for qualitatively judging the accuracy of the registration.

The robust behavior of the previously developed mutual information for automatic multimodality image fusion (MIAMI Fuse) registration algorithm (Meyer et al. 1997) for these pairs of same-modality, *i.e.*, ultrasound, data sets was a pleasant surprise. No preprocessing of the data sets, such as speckle reduction, was necessary, and the resulting registrations were of excellent quality and were obtained in relatively short times. Even the demanding task of warping using nine control points, *i.e.*, 27 degrees of freedom, yielded accurate, repeatable registrations, a feat even the authors initially considered as unlikely.

REFERENCES

Collignon A, Maes F, Delaere D, et al. Automated multimodality image registration using information theory. In: Viergever MA, ed. Computational imaging and vision, vol. 3. Ile de Berder: Kluwer Academic Publishers, 1995:263–274.

Fenn R, Fowlkes J, Moskalik A, et al. A hand-controlled, 3-D ultrasound guide and measurement system. In: Lees S, ed. Acoustical imaging, vol. 22. New York: Plenum Press, 1997;237–242.

Maintz J, Viergever M. A survey of medical image registration. Med Image Anal 1998;2:1–36.

Meyer CR, Boes JL, Kim B, et al. Demonstration of accuracy and clinical versatility of mutual information for automatic multimodality image fusion using affine and thin plate spline warped geometric deformations. Med Image Anal 1997;3:195–206.

Papoulis A. Probability, random variables, and stochastic processes. New York: McGraw-Hill, Inc., 1984.

Press WH, Flannery BP, Teukolsky SA, Vetterling WT. Numerical recipes in C: The art of scientific computing. Cambridge: Cambridge University Press, 1988.

Studholme C, Hill DLG, Hawkes DJ. Automated 3D registration of MR and PET brain images of the head by multiresolution optimization of voxel similarity measures. Med Phys 1997;24:25–35.

Viola P, Wells WM. Alignment by maximization of mutual information. 5th Int'l. Conf. on Computer Vision, vol. 95CH35744, IEEE, MIT, 1995:16–23.

Wells W, Viola P, Atsumi H, Hakajima S, Kikinis R. Multimodal volume registration by maximization of mutual information. Med Image Anal 1996;1:35–51.

Examples of 3-D Image Registration for Multimode, Extended Field of View, and Sequential Ultrasound Imaging

Jochen F. Krücker, Dipl.-Phys., Gerald L. LeCarpentier, Ph.D., Charles R. Meyer, Ph.D.,
Marilyn A. Roubidoux, M.D., J. Brian Fowlkes, Ph.D., Paul L. Carson, Ph.D.

Department of Radiology
University of Michigan Medical Center
Ann Arbor, MI, USA

Correspondence:
Paul L. Carson, Ph.D.
University of Michigan Medical Center
Department of Radiology
Kresge III, R3315
200 Zina Pitcher Place
Ann Arbor, MI 48109-0553
Vox: (734) 763-5884
Fax: (734) 764-8541

[Next: Abstract]

Examples of 3-D Image Registration for Multimode, Extended Field of View, and Sequential Ultrasound Imaging

Jochen F. Krücker, Dipl.-Phys., Gerald L. LeCarpentier, Ph.D., Charles R. Meyer, Ph.D., Marilyn A. Roubidoux, M.D., J. Brian Fowlkes, Ph.D., Paul L. Carson, Ph.D.

Abstract

Several potential uses of image registration and new display techniques in 3-dimensional ultrasound imaging are demonstrated in three examples, representing several types of applications: First, the gray-scale information of a color-flow image set was coregistered with a high resolution gray-scale set covering the same region of interest. The high accuracy achieved in this registration suggests that this technique can create improved images from combined ultrasound modes. Second, several parallel, partly overlapping gray-scale scans of a female breast with several lesions were coregistered and combined into one larger volume. Only in this extended field of view could the lesions be viewed simultaneously and their relative sizes and positions be appreciated, suggesting the potential of better detection of changes in breast regions being followed for potential cancer. Third, the image registration was applied to a series of ultrasound breast exams for cancer therapy assessment. In spite of considerable tumor shrinkage between the two scans obtained several weeks apart, the coregistration mapped the dominant features in the region of interest and thus facilitated tracking of changes over time, both with direct comparison and with displays that highlighted changes. The quality of the semiautomatic coregistrations achieved and the significance of the applications demonstrated here indicate that image registration may become a valuable tool in improving ultrasound diagnostics.

Introduction

Image registration or coregistration, the alignment of two or more 2-dimensional (2-D) or 3-dimensional (3-D) images of an object, has been applied to medical imaging for more than ten years. One major application of medical image registration is fusion of morphological images such as magnetic resonance imaging (MRI) and X-ray computed tomography (CT) with functional studies such as positron emission tomography (PET) and single photon emission computed tomography (SPECT) (1-7). Other applications of coregistrations include motion detection (8, 9), subtraction imaging (10, 11), and treatment planning (12, 13). A comprehensive review of different approaches and techniques in medical image matching can be found in (14).

Until recently, ultrasound image registration has not been successful, partly because of the small 2-D field of view and possibly strong tissue motion and deformation which make it difficult to obtain consistent image pairs for coregistration using conventional manual scanning.

With the advent of 3-D sonography in research (15, 16) and, more recently, in commercially available ultrasound scanners, volumetric ultrasound data have become available and can, in principle, be registered like 3-D data sets from other imaging modalities. However, the speckle noise and image artifacts usually present in ultrasound images and the strong angular dependency of the apparent brightness of specular reflectors challenge the robustness of registration algorithms.

Apparently the first successful coregistration of 3-D ultrasound scans in a phantom and in the breast was reported in (17), using registration software that required user definition of homologous points, lines, and planes in the data sets. Semiautomatic coregistrations of ultrasound scans were achieved very recently (18, 19) using software based on the mutual information (MI) of two data sets. The same software was used in this study to demonstrate three examples of potential applications of coregistration in ultrasound breast imaging. The display possibilities in this electronic medium, especially the movie features, should allow better visualization of registration quality and assessment of errors than conventional journals.

The gray-scale image obtained along with the color information in Doppler modes usually suffers from poor spatial resolution compared to the high resolution obtainable in the gray-scale-only mode. After registration of a 3-D Doppler mode data set with a gray-scale set, the color information can be superimposed on a high resolution gray-scale background, thus extracting the best of both imaging modes. Potentially, this allows more accurate diagnosis and higher sensitivity in lesion detection by displaying flow information in place with a high quality gray-scale image.

The small field of view (FOV) usually covered by a high resolution scanhead may be insufficient to use the full capabilities of 3-D ultrasound to detect and track changes in breast regions being screened or followed for possible lesions or response to treatment. Often the FOV is also too small to use the full advantages of 3-D in displaying morphologic distortions of normal tissue and flow surrounding the mass and differences between the possible mass and a statistically robust sampling of surrounding tissues. To create a complete or more complete image of the breast, the small volume covered by a single scan can be extended by repeatedly scanning the breast in parallel, partially overlapping sweeps which can then be combined using coregistration of the overlap. Compared to a commercially available 2-dimensional extended filed of view approach (20, 21), our Extended Volume Imaging (EVI) allows much faster acquisition of 3-dimensional volumes and is applicable as a post-processing scheme after the individual scans have been obtained.

In ultrasound screenings of the breast, some malignant changes are manifest as changes in echogenicity, texture, and morphology. Early detection of these changes can improve survival rates (22). Changes in a structure's size or shape can also aid detection of a malignancy or give important feedback in serial ultrasound exams for the assessment of response to cancer therapy. Coregistration of 3-D ultrasound exams can facilitate the temporal tracking of changes by coregistering the suspect regions of interest imaged at different times, thus allowing direct comparison of the 'before' and 'after' texture and morphology.

Materials and Methods

A LOGIQ 700 ultrasound scanner (**GE Medical Systems**, Milwaukee, WI) with a 12 MHz 1.5-dimensional matrix linear array probe was used to obtain 3-D data sets of the breast. The probe was mounted in a holder that restricted it to a linear motion in the elevational direction (perpendicular to the image plane) while electronically encoding the linear position of the probe in that direction. A more detailed description of the data acquisition scheme can be found in (23).

The holder was placed on the breast and the transducer slowly moved by hand over the region of interest. The high resolution gray-scale (GS), frequency-shift (f-CDI), and power-mode color Doppler (p-CDI) images obtained were then interpolated and resampled with a uniform elevational spacing of approximately 0.4 mm using the position data stored along with the images. Display and registration of the data sets were performed using AVS/5 and AVS/Express (**Advanced Visual Systems**, Waltham, MA).

The 3D image registration software **MIAMI Fuse** was originally developed for fusion of data sets from multiple imaging modalities including various combinations of MRI, CT, PET, and SPECT.

To define the approximate relative position of the two data sets to be coregistered, three control points have to be defined in each set. This is usually done by assuming the images were obtained in the same location and in the same orientation and requires very limited user interaction. The algorithm then repeatedly performs geometrical transformations, rigid or full affine, on one of two sets and maps it onto the second set until the best fit between the two sets is found. Here, the mutual information (24, 25) of the data sets is used as a cost function to determine the quality of a fit. With more control points, warping transformations can be performed, but that was not done in this study. For a more detailed description of the algorithm and evaluation of its performance with PET/CT, PET/MRI and SPECT/CT multimodal data sets see (26). More details on the application of this image registration software to 3-D ultrasound data sets are given in (19).

The registration software was used here to demonstrate registration of 3-D ultrasound scans of the breast for three different applications. For each class of application, one typical case is displayed to demonstrate its potential value in ultrasound diagnostics.

All patient data were acquired after informed consent was obtained.

1. The first application is the fusion of color information from Doppler imaging modalities with gray scale information from a high resolution gray-scale scan of the same volume. For this purpose, the right breast of a forty year old female patient was scanned in f-CDI mode and, several minutes later, in high resolution gray-scale mode, using average elevational frame spacings of 0.43 mm and 0.47 mm, respectively. The gray-scale information of the two scans was then coregistered and displayed in various ways to evaluate the goodness of match.

2. Extended Volume Imaging is the second application demonstrated in this study. Three parallel, high resolution gray scale scans were obtained in the left breast of a 65 year old woman diagnosed with a 60 mm invasive ductal carcinoma. The relative position and alignment of the scans is shown schematically in **Figure 1**. Starting with a scan in the center of the region of interest (B, average elevational frame spacing 0.32 mm), the 4 cm wide aperture of the transducer was then shifted 1 to 3 cm medially (A, frame spacing 0.29 mm) and laterally (C, frame spacing 0.37 mm), respectively, before the second and third scans. Thus, 3-D data sets with 25% to 75% overlap (AB, BC) were obtained. Volume registration was then performed on the overlapping regions to find the necessary transformations and exact relative positions of the data sets, mapping scan A and C into the reference frame given by scan B.

Note that our hardware does not encode the lateral position of the transducer, and that image-based methods, such as our volume registration, are preferable to hardware-encoded position since the image may be distorted by tissue motion or refraction artifacts. These distortions would be undetected by an external position encoder and could therefore lead to discontinuities in the extended image.

Three parallel, high resolution gray scale scans were obtained in the left breast of a 65 year old woman diagnosed with a 60 mm invasive ductal carcinoma. The relative position and alignment of the scans is shown schematically in **Figure 1**. Starting with a scan in the center of the region of interest (B, average elevational frame spacing 0.32 mm), the 4 cm wide aperture of the transducer was then shifted 1 to 3 cm medially (A, frame spacing 0.29 mm) and laterally (C, frame spacing 0.37 mm), respectively, before the second and third scans. Thus, 3-D data sets with 25% to 75% overlap (AB, BC) were obtained. Volume registration was then performed on the overlapping regions to find the necessary transformations and exact relative positions of the data sets, mapping scan A and C into the reference frame given by scan B.

Note that our hardware does not encode the lateral position of the transducer, and that image-based methods, such as our volume registration, are preferable to hardware-encoded position since the image may be distorted by tissue motion or refraction artifacts. These distortions would be undetected by an external position encoder and could therefore lead to discontinuities in the extended image.

Figure 1. The diagram shows the relative positions of three individual scans A, B, and C, combined into one extended 3-D field of view. The three scans are approximately parallel and overlap at least 25% to achieve sufficient accuracy in the coregistration. Scan B serves as a reference, the overlap AB is used to align scan A relative to B, and similarly BC is used to align C relative to B.

3. The third application presented in this article is the registration of ultrasound

Results

1. Multimodal Ultrasound Imaging

   Figures 2 and **3** show the results of registering a 3-D f-CDI volume with a high resolution gray-scale volume. The two image volumes were acquired sequentially during a single patient visit. The forty year old female patient was diagnosed with right infiltrative ductal carcinoma. Note the 13 mm spiculated mass which appears in both **Figures 2(b)** and **3** (white arrow).

<div align="center">

(a)   **(b)**   **(c)**

</div>

Figure 2. Composite representation of an f-CDI volume coregistered with a high resolution gray-scale volume. The high resolution gray-scale images are pseudo-colorized from blue (weak echo) to red (strong echo) and superimposed onto the gray-scale of the f-CDI set. The scans were performed minutes apart. **(a)** Three orthogonal planes of the 3-D coregistered volume. The white labels indicate our naming scheme for the three planes. **(b)** Axial-lateral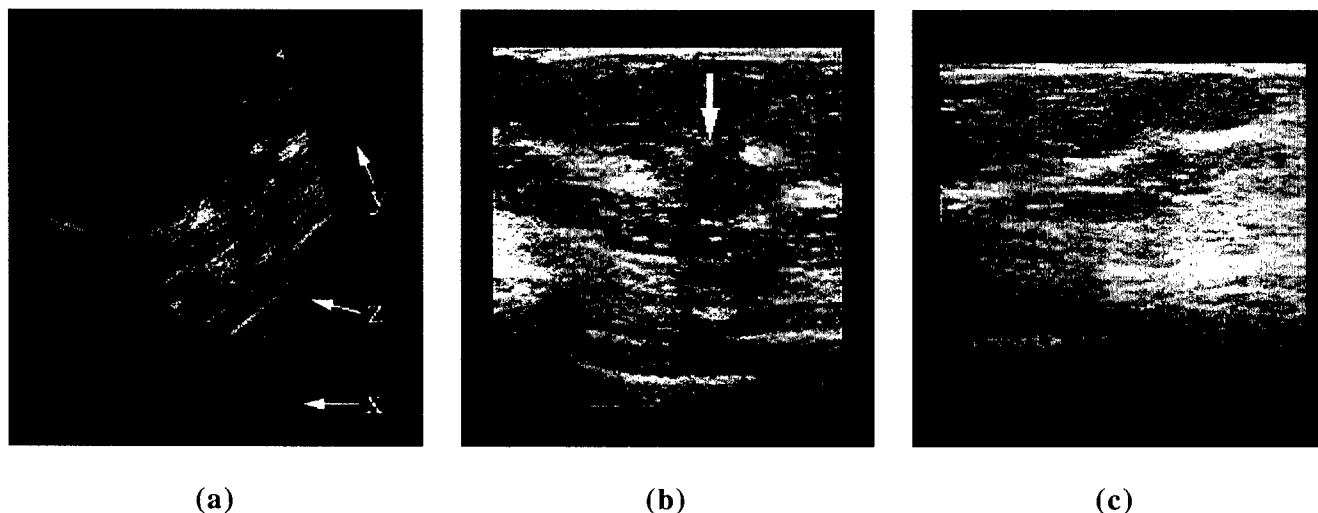 (z) scan plane. The white arrow points at the 13 mm spiculated mass. **(c)** Axial-elevational (x) transverse plane. Click each image to view its full sized counterpart. Click **here** for a Quicktime movie (444 kB) scanning through the entire volume and containing the frames shown in **(a)-(c)**. For a high-quality version of the same movie (1.2 MB), click **here**.

   In **Figure 2**, the volumetric data is shown as composite images of the f-CDI and the high resolution gray-scale scans. **Figure (a)** displays three orthogonal planes of the 3-D volume, **(b)** and **(c)** display the axial-lateral and axial-elevational planes, respectively. The gray-scale component of the f-CDI is represented with a "gray-scale" map, while the high resolution gray-scale is colorized by the blue-green-yellow-red spectrum, representing dark to light echo regions. The two image sets are then superimposed onto each other. Note the overlap of features in all three images of the figure, with reds and yellows overlapping the lighter features. To view a Quicktime movie (444 kB) scanning through the entire volume, click **here** or follow the link in the figure caption.

   In **Figure 3**, the particular scan plane shown in **Figure 2(b)** is presented in a different way. In this case, the coregistered planes are not combined into a composite view. Rather, a diagonal line separates the gray-scale from the f-CDI (upper left) from the high resolution gray-scale image (lower right). The viewer is then able to see the alignment of various features at the diagonal boundary for comparison. Note that the sharp borders of the spiculated mass (white arrow) clearly visible in **Figure 3(b)** are barely discernible in the gray-scale from the f-CDI image shown in **Figure 3(a)**. In a Quicktime "wiper" movie (348 kB), the viewer can appreciate both the accuracy of the registration as well as the sharpness of the high resolution gray-scale over that of the f-CDI view by sweeping the border back and forth over the suspicious region. Again, click **here** for the movie or follow the link in the caption.

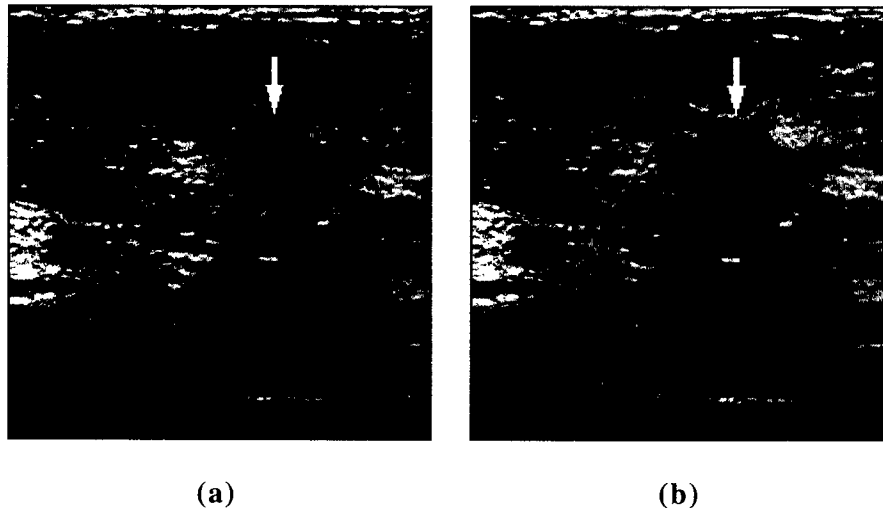**(a)**   **(b)**

Figure 3. Lateral-axial scan plane shown in **Figure 2(b)**. In both images, the left of the diagonal line shows the gray-scale from the f-CDI while the lower right shows the high resolution multifocal gray-scale image. **(a)** More of the lower resolution image is shown. Note the alignment of various structures at the diagonal image boundary. **(b)** In this view, more of the high resolution gray-scale is shown. Note the detectability of the spiculated mass (white arrow) just to the right of the diagonal line in the upper portion of the image. In **(a)** this structure is barely discernible. Click either image to view its full sized counterpart. Click **here** for a full Quicktime "wiper" movie (348 kB) containing the frames shown in **(a)** and **(b)**.

Even if the mapping of the two image sets displayed above appears to be very accurate, close inspection of the data reveals a small remaining error in the alignment of discernible landmarks. The main causes of error appear to be

1. Local tissue motion and deformation as caused by respiratory motion and compression of superficial tissue by the transducer itself. These local deformations can be corrected only in part by the global geometric transformation applied here to register the two data sets.

2. Noise in the image sets or any other inherent differences between the sets to be registered as introduced by employing different imaging modes or modalities (here: gray-scale and f-CDI ultrasound).

3. Changes in look direction which cause changes in the apparent brightness of specular reflectors since the echo received from specular reflectors strongly depends an the angle of incidence of the ultrasound pulse. Even if very apparent to the eye, this may actually only be a minor cause of misalignment since the volume covered by specular reflectors is small compared to the total volume, and thus the mutual information affiliated with it contributes little to the maximization of the total mutual information.

The quality of the registration was evaluated by a single observer as described above. The mean alignment error obtained, based on 13 manually defined common landmarks, was 1.1 mm. It should be noted that this value depends on the position and distribution of the selected points throughout the volume and is somewhat subjective. The peak alignment error estimate was 2.9 mm on the left side of the image near the chest wall whose movability is unrelated to the transducer pressure applied.

2. Extended Volume Imaging

Figure 4 displays the extended 3-D field of view of an invasive ductal carcinoma scanned in a 65 year old woman. The orientation and relative position of the three scans used to form this extended volume was described

in **Figure 1**. In this particular example, the central (B) and medial (A) scans overlapped about 75%, the central and lateral (C) scans overlapped 25%, resulting in a total width of the extended field of about 7.9 cm. In **Figure 4**, the boundaries between the displays of the coregistered scans at 0.3 and 0.6 of the total width of the extended volume, marked by white arrows in the 2-D view of **Figure 4**, are hardly noticeable. Note that no averaging or other processing (other than slight image compression for on-line display) was employed at the boundaries to smooth out the transition. The display changes abruptly from scan A to B and from B to C, which makes the continuous appearance of the extended view even more remarkable.

A Quicktime **movie** (548 kB) can be displayed for appreciation of the quality of the composite view throughout the volume.
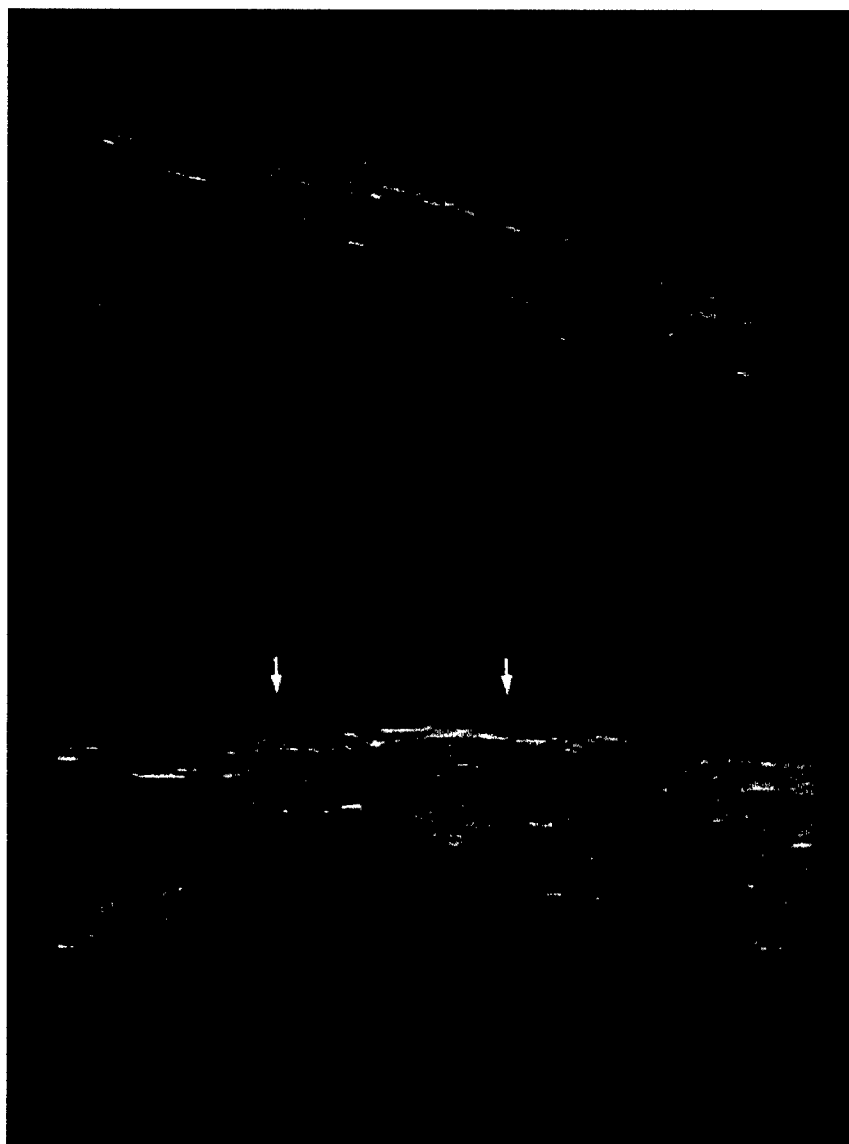
Figure 4. (Top) 3-D view of a volume combined from three parallel, partly overlapping scans in a 65 year old female with invasive ductal carcinoma. (Bottom) 2-D view of the axial-lateral plane displayed in the volume above. The width of this extended view is 7.9 cm. The boundaries between the original scans at about one third and two thirds of the width of the composite image (white arrows) are hardly noticeable. Click **here** for a Quicktime movie (548 kB) displaying an elevational sweep through the extended volume. For a high-quality version of the same movie (1.3 MB), click **here**.

In this example, commercially available high-resolution transducers, with aperture widths of typically four cm,

could have only fully displayed one of the masses at a time. This limitation may make the visualization and evaluation of the entire structure using ultrasound more difficult. In the extended view, the three distinct masses are displayed simultaneously in their relative positions as determined by the coregistration in the overlapping regions. This allows immediate perception of the entire region of interest and reveals more of the overall anatomy and anatomical relationships. The large FOV should also diminish the danger of missing important details at the edges and facilitate measurements within the extended volume.

The remaining misalignment of the registered scans in the overlapping regions, based again on visual inspection of identifiable structures and measurement of their apparent shift, was estimated to be 0.8 mm mean (1.5 mm peak) in the 75% overlap region and 1.4 mm mean (3.1 mm peak) in the 25% overlap region.

3. Sequential 3-D Imaging

Figure 5 shows an example of a coregistration of sequential scans of a breast lesion in a patient undergoing CAF chemotherapy. The 65 year old woman had a palpable 2.5 cm mass and was later diagnosed with left invasive ductal carcinoma with a focal mucinous carcinoma component. The two scans displayed here were acquired 8 days before and 29 days after the start of the chemotherapy. Two more scans, obtained and coregistered 55 and 78 days, respectively, after the start of the therapy, yielded similar registration results and are not displayed here.

Although the size and shape of the lesion changed significantly between the first two scans, the registration procedure aligned the lesions well and allows better comparison and visualization of changes than without registration.

(a)

(b)
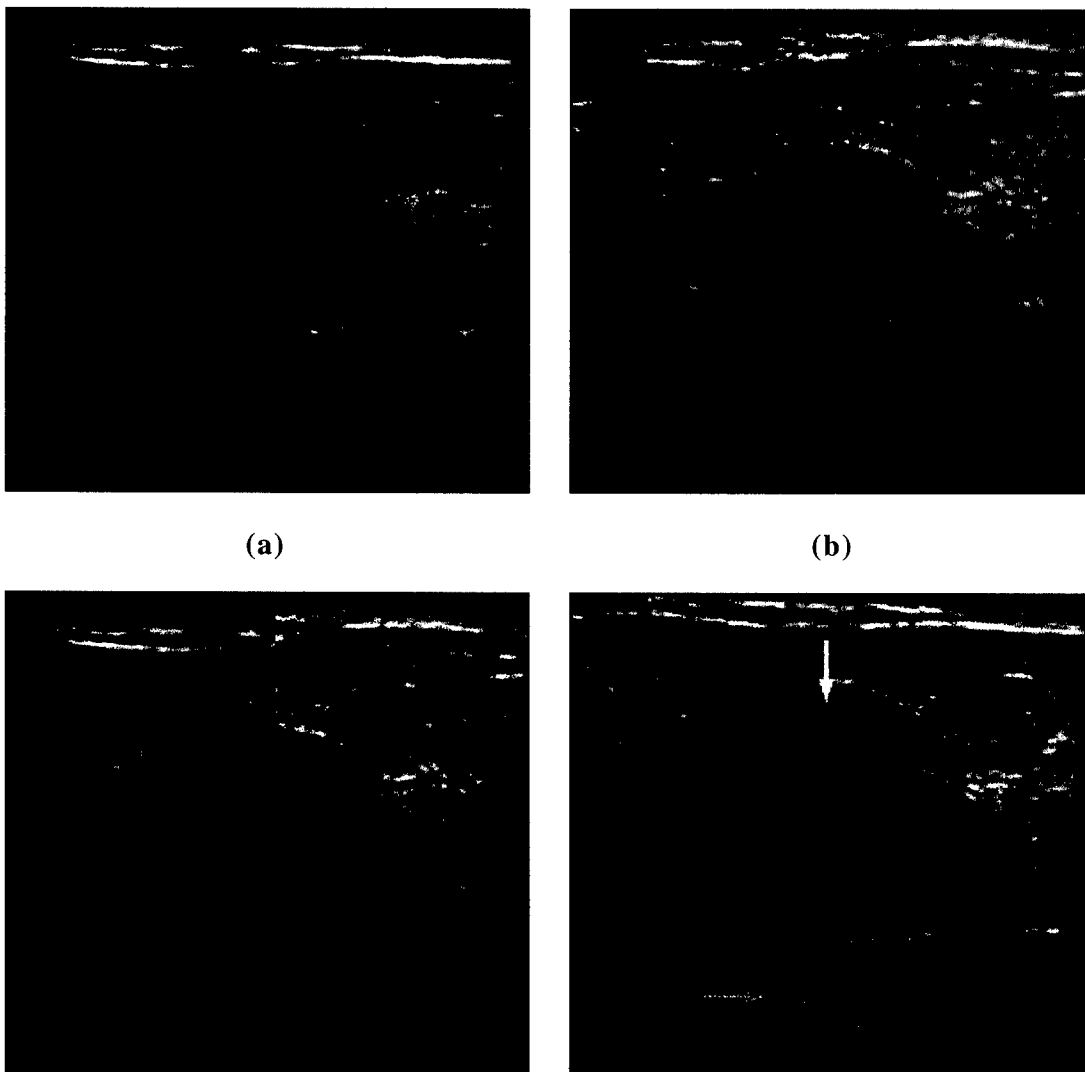
(c)   **(d)**

Figure 5. Coregistration of two sequential scans of a breast lesion in a patient undergoing chemotherapy. **(a)** Central B-scan frame of the first scan, obtained one week before the start of the therapy, coregistered and transformed to map onto the second scan. **(b)** Corresponding frame of the second scan, obtained 5 weeks later. **(c)** Combined view of the same frame in the first (left) and second scan (right). Click **here** for a Quicktime "wiper" movie (304 kB) showing the temporal changes throughout this frame by moving the border between the scans from left to right. **(d)** Pseudo-color image of the differences between the two scans, showing increased echogenicity (blue) where the mass shrank (white arrow), and decreased echogenicity (yellow) below the mass (gray arrow). Click **here** for a 292 kB movie displaying the differences throughout the scanned volume.

Figure 5(a) and **(b)** show corresponding frames from the center of the first and second scan, respectively, after coregistration of the volumes. In this case, the first scan was transformed using a full affine transformation to map onto the second one. In a serial study with scans obtained manually and several weeks apart, small changes in look direction or positioning of the transducer are unavoidable even if the sonographer carefully tries to reproduce the field of view of a previous scan. These variations can make direct comparison of two serial scans more difficult. However, if the two scans have enough common information, the registration software can detect these changes and transform one set accordingly. Hence, the slight rotation of the image in **(a)** can be understood as a correction for a small change in view direction between the two scans.

Figure 5(c) shows a combined view of the frames displayed in **(a)** (left half) and **(b)** (right half of the image), which reveals the change in size and other characteristics of the lesion. Also seen is a small error in aligning the specular reflectors at the top of the images, assuming the same tissue planes are producing the specular reflections in the two scans. This near field error is most likely induced by a local deformation of the tissue by the pressure of the transducer against the skin. The estimation of the average misregistration in this serial study is difficult and prone to error because of the additional effect of drug-induced changes over time. These changes cannot be unambiguously separated from the other causes of registration error as discussed above. However, estimating the average error by identification of corresponding landmarks in the two registered sets well outside the tumor volume, a mean error of 1.4 mm (peak 2.2 mm) was obtained.

For better visual evaluation of the registration quality and change in tumor size, a Quicktime movie (304 kB) can be viewed by clicking **here** or on the link in the caption of **Figure 5(c)**. In the movie, the border between the two scans as displayed in **(c)** can be moved from left to right, thus revealing more of the first or the second scan.

In **Figure 5(d)**, the change in tumor size is highlighted using a pseudo-color display. By simultaneously feeding the gray-scale values of the coregistered first scan into the red and green channels of a RGB (red, green, blue) display and the gray-scale values of the second scan into the blue channel of the same display, a difference image is created with a color map from yellow (echogenicity of first scan larger) through gray (echogenicities identical) to blue (echogenicity of second scan larger). The saturation of the colors is proportional to the difference in gray-scale value, i.e. the larger the difference, the stronger the color. The shrinkage of the hypoechoic mass causes an increase in echogenicity on the mass periphery in the second scan compared to the first. This difference is clearly visible as a blue rim (white arrow) surrounding the proximal half of the mass in **(d)**. The distal part of the mass shows no such blue rim and therefore appears to be unchanged. This may be explained by the surrounding anatomy which can cause asymmetric tissue deformation and displacement around the shrinking mass.

The other prominent feature in this figure is the yellow area immediately below the tumor (gray arrow), indicating an area of decreased echogenicity. This decrease could be explained by a mostly blood-filled mass which has lower attenuation than the surrounding tissue and thus causes an apparent enhancement below the mass. The smaller mass in the second scan then causes less enhancement and therefore a decrease in echogenicity, which can also be seen by comparing **Figures 5(a)** and **(b)**, but which is more obvious in the color display of **(d)**.

By clicking **here** or on the link in the caption of **Figure 5(d)**, a movie (292 kB) can be displayed showing the difference image of **(d)** for 47 frames of the scanned volume. Note the shrinkage of the mass in all 3 dimensions by following the blue rim throughout the movie. Quantitative evaluation of the entire scans using polygons to manually define the border of the lesion in each frame yielded a reduction in lesion volume of approximately 27%.

4. Reproducibility of Results

More examples have to be registered to study case-to-case variations in accuracy, and factors limiting the function of the registration algorithm. So far, two examples of multimode registration, five extended volumes, and five sequential cases have been studied. By visual assessment, the two multimode registrations were of similar quality. Also, four of the sequential cases were of comparable registration quality. In a fifth case, no registration could be found. Visual inspection showed that either the sonographer had not scanned enough of the same volume in the two sequential scans, or the mass had disappeared completely in response to treatment. In extended volume studies, four out of five cases were similar to the one displayed here. In the fifth case, the overlap was less than 1 cm and no acceptable registration was found.

Discussion

The examples described are successful and significant applications of image registration in 3-D ultrasound. They demonstrate the feasibility of a new technique to improve ultrasound diagnostics and potentially open a new range of related applications.

Routine coregistration and combination of image sets obtained using a variety of different ultrasound modes or using ultrasound and a second imaging modality should be possible with the same or only slightly modified version of the currently used registration software.

In ultrasound multimode imaging, the coregistration should allow image optimization, i.e. replacement of a lower quality component of one image set with the higher quality component of a different set, as in the substitution of high resolution gray-scale data for the lower resolution gray-scale 'background' of color flow imaging modes, as well as image fusion, i.e. the combination of images displaying different physical properties, which increases the diagnostic value of either one of the original images by relating one physical property to another. Note that the reduced quality of the image in CDI mode compared to gray-scale mode is due to natural timing constraints in image formation, and is therefore likely present to some extent in most or all modern ultrasound scanners. The difference is probably more marked here because the matrix array used allows more image improvements in the gray-scale images that cannot be realized in CDI modes than usually possible with 1-D arrays.

Possible modes for image fusion can include, but are not restricted to, frequency-shift and power mode Doppler, harmonic imaging, and new modes being researched and developed such as imaging with contrast agents or ultrasound elasticity imaging (27, 28). The quality of the registration will depend on the information content of the images, more specifically, the mutual information. Where only gray-scale information was employed for the registration, the accuracy did not allow an exact pixel by pixel match, but the registration was far better than can be done manually.

In multimodal imaging, coregistrations of ultrasound scans with MR, CT, and other 3-D data sets, or with projection images such as mammograms can be envisioned. If ultrasound scans are obtained in the same or a similar geometry as for a mammogram, a coregistration of a projection of the ultrasound scan with the mammogram could combine the most inexpensive and commonly used modalities for breast imaging. This would add 3-D information to the 2-D mammogram and allow more accurate tracking of spots identified in the mammogram using 3-D ultrasound.

Extended Volume Imaging is a method to overcome one of the major disadvantages of ultrasound imaging compared to most other modalities: the very limited field of view and unsystematic coverage of the region of interest. In breast imaging, a wider field of view should be particularly desirable in following suspicious regions and in detection of preclinical disease. To follow in 3-D the morphology of a large lesion and its effect on the surrounding tissue, a larger field of view will be essential. A combination of Extended Volume Imaging and multimode (gray-scale and CDI) imaging would even allow tracking of vascular and tissue morphology simultaneously in high quality images. Screening of women at very high risk for breast cancer is beginning to draw more interest in the US with incidental detection of malignant foci at locations removed from the site of suspicion (29). Accordingly, Extended Volume Imaging is likely to increase the sensitivity of ultrasound in breast cancer detection. A wider field of view will also help in covering previously scanned sites and thus determining changes over time, either in screening of high risk groups, tracking suspicious regions, or monitoring response to treatment. While radiologists and sonographers can reach very high skill levels, it is often difficult for some operators to assure that the same views are obtained in two or more serial studies. Interpretation is also complicated when the interpreter has not personally performed the exam. Both problems could be reduced using Extended Volume Imaging.

The accuracy of coregistrations of partly overlapping volumes appears to depend on the size of the overlap. It is possible that the larger the overlap, the more common structure is available to align the scans, and the less the registration algorithm is potentially affected by noise. The minimum overlap required for acceptable registration accuracy can vary with the information content of the data sets. However, in the examples studied so far, a 1 cm (25%) overlap generally produced acceptable registrations, judged by visual inspection.

Coregistration of sequential exams may enhance manual (visual) detection of changes in several ways, and may eventually allow for semiautomatic or automatic volume change estimations. First, the registration corrects for slight changes in scan position and direction, and thus allows direct comparison of the same areas imaged at different times. This may resolve ambiguities in the actual location of the scans and may also help detecting subtle

changes that go unnoticed in unregistered scans. Second, registered sequential scans enable new display techniques that emphasize changes between scans, such as the difference image shown in **Figure 5(d)**. Using this type of difference image may enhance and accelerate the detection of changes, and it may ultimately be possible to segment regions of shrinkage and growth for rapid, semiautomatic volume change estimations. Third, if the registration is predominantly based on a mass and its boundaries, and if non-rigid linear or non-linear transformations are used, the registration could map the boundaries at one point of time to the boundaries at another point of time. The transformation matrix itself then contained information about size changes and could also be used for semiautomatic volume change estimations. Note also that the registrations can be obtained semiautomatically and with very limited user interaction. Manual registration in 3-D by visual comparison of two volumes may be possible, but is a time-consuming and tedious process, and subject to user variability.

For serial exams, the Extended Volume Imaging technique might be combined with coregistration of scans obtained at different times. This would allow the visualization and quantification of changes in large lesions over time. In fact, the acquisition and composition of an extended field of view might prove to be necessary for tracking rapidly changing, large lesions because in this case a small field of view might not contain enough unchanged structure (which is usually found well outside the volume of the mass) for the coregistration to work properly. If routinely used in serial exams of women with high risk of breast cancer, coregistration could help detect early changes not apparent in multiple small FOV scans, thus increasing the chances of effective treatment.

For validation of quantitative measurements made in coregistered image sets, an automated error estimation is desirable. The quality of coregistrations can vary strongly with the available mutual information, which depends on the amount of shadowing, specular reflectors, and local tissue deformation present in the image sets. Manual evaluation, as in the examples presented here, may not be practical to assure accuracy of quantitative measurements of dimensions over long distances.

A variety of automatic evaluation techniques can be envisioned and will be explored and compared with each other and with manual evaluation to find the most accurate and practical method.

An accuracy measure similar to the average alignment error obtained manually can be computed by splitting up the two registered volumes into a number of subvolumes and performing an iterated registration on each of the pairs of subvolumes, using simple rotate/translate or full affine transformations. Since the subvolumes are already approximately aligned, the control points for the second registration can be placed automatically and do not require user interaction. Assuming that the main cause of error in the initial registration is local tissue deformation unaccounted for by the global deformation model applied, an iterated registration on small subvolumes should greatly increase the accuracy of the alignment. If the remaining error after the second registration is assumed to be small compared to the initial error, the registered subvolumes can be used as a reference representing 'true' alignment. The mean translation vector of all subvolumes from their positions after the first registration to their position after the second registration can be used as an estimate of the average alignment error. Compared to the manually obtained estimate it will have the advantage of covering the entire volume and being almost user independent.

Alternatively, instead of splitting up the volume and performing linear geometric transformations on each subvolume, a reference registration employing a global non-linear transformation can be obtained. The data sets can be registered with a warping transformation defined by an increasing number of control points until the mutual information of the final registration converges. Thus the mean warping distance of the final transformation can be used as another estimate of the alignment error after the initial registration.

Both manual and automatic estimation of average alignment errors can be validated in phantom scans using tissue phantoms with an additional, known distribution of point reflectors. The point reflectors are common landmarks in the registered sets that can be unambiguously identified, thus enabling a very accurate manual error estimation that can serve as a gold standard. For the registration procedure, the point reflectors have to be deleted from the digitized data sets (replaced by zero values), otherwise they would provide additional information that leads to better registrations than in the tissue phantom alone. The same data sets (with the point reflectors removed) can be used for both manual and automatic error estimation and compared to the gold standard based on the original data sets.

A problem with phantom studies is the difficulty in accurately simulating breast tissue including phase aberrations and tissue deformability. Current phantoms known to the authors do either not exhibit the aberrations present in real breast tissue, or are much less deformable than breast tissue (30). As a result, the registrations obtained in phantoms might be more accurate than *in vivo* breast scans and therefore be unsuited as gold standard.

The accuracy information also helps to determine which kind of mapping transformation is needed to provide

clinically useful registrations. In this study, only global linear (full affine) transformations were employed. In cases with strong local tissue deformation, non-linear warping transformations might be required to keep the registration error low. With warping, the registration algorithm may locally deform the 3-D image set in order to map deformed tissues. Initial studies showed that including non-linear transformations can increase the mapping accuracy significantly (31).

In future studies, the techniques developed here in breast scans could also be applied to scans of other organs. Since phase aberrations and tissue deformability, which introduce registration errors, are particularly strong in breast, registrations in liver, kidney, prostate and other organs are likely to be at least of similar quality compared to the examples shown here.

References

1. Pietrzyk U, Herholz K, Heiss WD. Three-dimensional alignment of functional and morphological tomograms. J Comput Assist Tomogr 1990; 14(1):51-9

2. Alpert NM, Bradshaw JF, Kennedy D, Correia JA. The principal axes transformation--a method for image registration. J Nucl Med 1990; 31(10):1717-22

3. Faber TL, McColl RW, Opperman RM, Corbett JR, Peshock RM. Spatial and temporal registration of cardiac SPECT and MR images: methods and evaluation. Radiology 1991; 179(3):857-61

4. Loats H. CT and SPECT image registration and fusion for spatial localization of metastatic processes using radiolabeled monoclonals. J Nucl Med 1993; 34(3 Suppl):562-6

5. Hill DL, Hawkes DJ, Gleeson MJ, et al. Accurate frameless registration of MR and CT images of the head: applications in planning surgery and radiation therapy. Radiology 1994; 191(2):447-54

6. Ardekani BA, Braun M, Hutton BF, Kanno I, Iida H. A fully automatic multimodality image registration algorithm. J Comput Assist Tomogr 1995; 19(4):615-23

7. West J, Fitzpatrick JM, Wang MY, et al. Comparison and evaluation of retrospective intermodality brain image registration techniques. J Comput Assist Tomogr 1997; 21(4):554-66

8. van Herk M, Bruce A, Kroes AP, Shouman T, Touw A, Lebesque JV. Quantification of organ motion during conformal radiotherapy of the prostate by three dimensional image registration. Int J Radiat Oncol Biol Phys 1995; 33(5):1311-20

9. Andersson JL. How to obtain high-accuracy image registration: application to movement correction of dynamic positron emission tomography data. Eur J Nucl Med 1998; 25(6):575-86

10. Yin FF, Giger ML, Doi K, Vyborny CJ, Schmidt RA. Computerized detection of masses in digital mammograms: automated alignment of breast images and its effect on bilateral-subtraction technique. Med Phys 1994; 21(3):445-52

11. Lehmann T, Sovakar A, Schmitt W, Repges R. A comparison of similarity measures for digital subtraction radiography. Comput Biol Med 1997; 27(2):151-67

12. Leszczynski KW, Loose S, Boyko S. An image registration scheme applied to verification of radiation therapy. Br J Radiol 1998; 71(844):413-26

13. Wilson DL, Carrillo A, Zheng L, Genc A, Duerk JL, Lewin JS. Evaluation of 3D image registration as applied to MR-guided thermal treatment of liver cancer. J Magn Reson Imaging 1998; 8(1):77-84

14. van den Elsen PA, Pol EJD, Viergever MA. Medical Image Matching - A Review with Classification. IEEE Eng Med Biol 1993; 12(1) 26-39

15. Candiani F. The latest in ultrasound: three-dimensional imaging. Part 1. Eur J Radiol 1998; 27 Suppl 2:S179-82

16. Campani R, Bottinelli O, Calliada F, Coscia D. The latest in ultrasound: three-dimensional imaging. Part II. Eur J Radiol 1998; 27 Suppl 2:S183-7

17. Moskalik A, Carson PL, Meyer CR, Fowlkes JB, Rubin JM, Roubidoux MA. Registration of three-dimensional compound ultrasound scans of the breast for refraction and motion correction. Ultrasound Med Biol 1995; 21(6):769-78

18. Meyer CR, LeCarpentier GL, Roubidoux MA, et al. Automated Coregistration of Three-Dimensional Ultrasound Volumes by Mutual Information: Sequential Examples of Breast Masses. (Proceedings of AIUM 42nd Annual Conference, Mar. 22-25) J Ultrasound Med 1998; 17:S1, S87.

19. Meyer CR, Boes JL, Kim B, et al. Semiautomatic Registration of Volumetric Ultrasound Scans. Ultrasound Med Biol (in press).

20. Weng L, Tirumalai AP, Lowery CM, et al. US extended-field-of-view imaging technology. Radiology 1997; 203(3):877-80

21. Kroger K, Massalha K, Dobonici G, Rudofsky G. SieScape: a new sonographic dimension with fictive images. Ultrasound Med Biol 1998; 24(8):1125-9

22. Sivaramakrishna R, Gordon R. Detection of breast cancer at a smaller size can reduce the likelihood of metastatic spread: a quantitative analysis. Acad Radiol 1997; 4(1):8-12

23. LeCarpentier GL, Tridandapani PB, Fowlkes JB, Moskalik AP, Roubidoux MA, Carson PL. Utility of 3D Ultrasound in the Discrimination and Detection of Breast Cancer. Submitted to RSNA Electronic Journal.

24. Maes F, Collignon A, Vandermeulen D, Marchal G, Suetens P. Multimodality image registration by maximization of mutual information. IEEE Trans Med Imaging 1997; 16(2):187-98

25. Kim B, Boes JL, Frey KA, Meyer CR. Mutual information for automated unwarping of rat brain autoradiographs. Neuroimage 1997; 5(1):31-40

26. Meyer CR, Boes JL, Kim B, et al. Demonstration of accuracy and clinical versatility of mutual information for automatic multimodality image fusion using affine and thin plate spline warped geometric deformations. Med Image Anal 1997; 1(3):195-206

27. Shapo BM, Crowe JR, Erkamp R, Emelianov SY, Eberle MJ, O'Donnell M. Strain imaging of coronary arteries with intraluminal ultrasound: experiments on an inhomogeneous phantom. Ultrason Imaging 1996; 18(3):173-91

28. Erkamp RQ, Wiggins P, Skovoroda AR, Emelianov SY, O'Donnell M. Measuring the elastic modulus of small tissue samples. Ultrason Imaging 1998; 20(1):17-28

29. Gordon PB, Goldenberg SL. Malignant breast masses detected only by ultrasound. A retrospective review. Cancer 1995; 76(4):626-30

30. Madsen EL, Kelly-Fry E, Frank GR. Anthropomorphic phantoms for assessing systems used in ultrasound imaging of the compressed breast. Ultrasound Med Biol 1988; 14 Suppl 1:183-201

31. Krücker JF, Meyer CR, Tuthill TA, LeCarpentier GL, Fowlkes JB, Carson PL. 3-D Compounding of B-Scan Ultrasound Images. Proceedings of the 137th regular meeting of the Acoustical Society of America, Berlin, 1999 (in press).

3-D Compounding of B-Scan Ultrasound Images

Jochen F. Krücker, Charles R. Meyer, Theresa A. Tuthill, Gerald L. LeCarpentier,
J. Brian Fowlkes, Paul L. Carson

University of Michigan, Dept. of Radiology, 200 Zina Pitcher Place *Ann Arbor, MI 48109, USA*

Summary: Two applications of volume registration in 3-D ultrasound imaging, extended volume imaging (EVI) and 3-D Spatial compounding, are demonstrated both in phantom and clinical scans. Extended volumes were composed by obtaining partly overlapping scans, registering the overlapping volumes, and displaying the complete set of volumes in their relative spatial orientations as determined by the registration procedure. 3-D compound images were created by scanning volumes from several elevational look directions, registering, and averaging the different views. In both applications, the volume registration worked accurately and provided significant image improvements.

INTRODUCTION

Image registration, or coregistration, can be used to combine several sets of images obtained with different imaging parameters or modalities, from different look directions, or at different times. In medical imaging, it has mainly been applied to magnetic resonance imaging, X-ray computed tomography, and tomographic nuclear imaging modalities. Recently it has been shown that some image registration techniques can also be used to register 3–D ultrasound data sets [1-3]. In this study, we demonstrate two registration-based examples of image enhancements in 3-D ultrasound: Extended volume imaging (EVI) and 3-D spatial compounding. With EVI, one of the major limitations of high-frequency ultrasound scanners, the small field of view, can be overcome. This application is particularly important in sequential ultrasound exams, e.g. in screening for breast cancer or following cancer therapy, where large fields of view are needed to locate areas of change and to make sure that the same area is covered in sequential scans. Spatial compounding can deliver improved images with reduced speckle noise and increased contrast-to-noise ratio. It also reduces shadowing, and creates more complete images of connective tissues and other specular reflectors.

MATERIALS AND METHODS

Since the registration algorithm we used is fully explained in [4] , we will only briefly describe the relevant features here. The software performs either affine, i.e. linear, geometric transformations to map one image volume onto another, or non-linear thin-plate spline (TPS) warpings. When using full affine transformations, the user places 4 initial control points in each data set. The control points define the approximate mapping transformation from one set (reference) onto another (homologous). By varying the position of the control points, the algorithm refines the transformation until the mutual information (MI) of the reference and the

transformed homologous set is maximized. The MI, defined as the difference between the sum of the individual entropies and the joint entropy of two random variables, thus serves as a cost function in this optimization problem. For warping transformations, the user defines at least one more control point and increases the degrees of freedom of the registration transformation with each additional control point. Note that no pre-processing, like cropping or speckle reduction, has to be applied to the image sets before registration.

A clinical ultrasound scanner (Logiq 700, GE Medical Systems, Milwaukee, Wis) with an 11MHz 1.5-dimensional linear matrix array probe was used for all data acquisition. With electronic elevational (normal to scan plane) focussing, the average axial and elevational resolution cell diameters were 0.31 mm and 0.72 mm, respectively[1]. The transducer was attached to a 2 degree of freedom position encoder that restrained the motion of the probe to linear elevational scanning and elevational tilting. The position information was used to uniformly interpolate and shear the raw B-scan image sets before volume registration. All phantom scans were obtained in a focal lesion phantom (CIRS; Computerized Imaging Reference Systems, Norfolk, Va). All clinical scans were obtained in the female breast.

To create extended volume images, the area of interest was imaged in 3 or 4 approximately parallel, partly overlapping scans (Fig. 1). If 3 scans were used, the central scan (B) served as a reference relative to which the outer scans (A, C) were registered by maximization of the mutual information in the overlaps, AB and BC. In cases where 4 scans were combined (A, B, C, and D), D was first registered relative to C. The combined volume (C&D) and volume A were then registered relative to the global reference B using the overlaps BC and AB.

EVIs were obtained both in phantom scans and clinical breast scans. In phantom scans, the registration accuracy in the extended lateral direction was evaluated by comparing the true position of 50 spheres (3mm diameter) in the phantom to the position found in the extended view. In clinical scans, the registered volumes were visually assessed and the position of common landmarks marked in each set. The average registration error was defined as the mean distance between point pairs defining common landmarks.
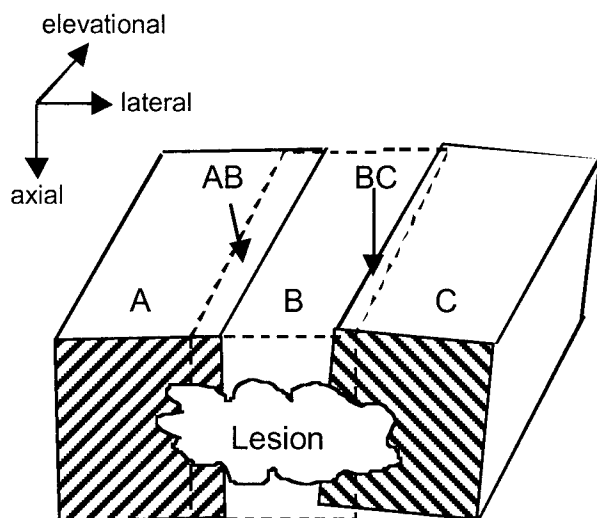

Figure 1: Extended Volume Imaging. Volumes A and C are registered relative to reference volume B.
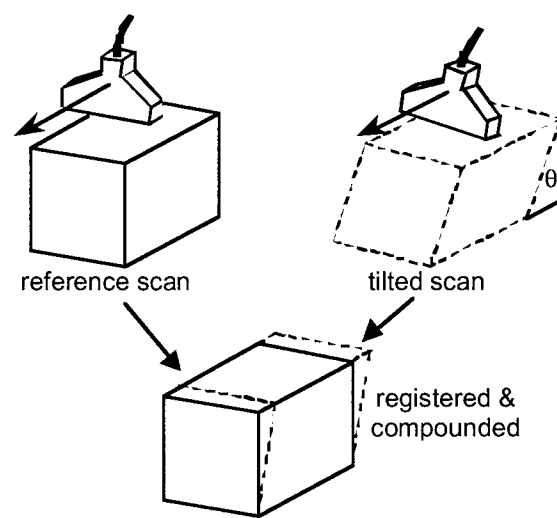
Figure 2: Spatial compounding of volumes obtained at different elevational tilt angles

---

[1] A phantom was scanned axially and elevationally in an area that produced fully developed speckle. The resolution cell diameters were defined as the standard deviation of the Gaussian fit to the frame-to-frame correlation functions.

For compound imaging, partly uncorrelated views were obtained by changing the tilt angle of the transducer before re-scanning the area of interest (Fig. 2). The interpolated and sheared image sets were registered using either full affine or warping transformations. The registered data sets were then log-decompressed, averaged, and recompressed to the same dynamic range as the original images (69 dB).

The registration accuracy in phantom scans was determined using a semiautomatic edge detection algorithm. Given the approximate center of a spherical hypoechoic area, the algorithm finds the exact center and the two radii on which the average signal increased 10% and 90%, respectively, of the difference between the maximum signal level outside the circle and the minimum inside. The difference between the radii will be referred to as the boundary width of the spheres. The accuracy in clinical compound scans was estimated by the same visual method used for clinical EVI.

RESULTS AND DISCUSSION

Figure 3 displays an example of an axial-lateral cross section through an EVI created from 4 partly (30%, 35%, and 58%) overlapping phantom scans registered with full affine transformations. No averaging or other processing was applied in the areas of overlap. The white arrows indicate the display boundaries between the registered original scans. Note the continuous appearance of specular reflectors across the boundaries and the spherical symmetry of voids placed on boundaries. The total width of the cross section is 10.6 cm. The average lateral deviation of the spheres in the extended volume from their true position is +0.47%.

EVI in clinical scans produced similar alignment quality as long as the breast was stabilized during the scans to keep local tissue deformation at a minimum [5]. The average distance of common landmarks identified in the registered overlaps ranged from 0.8 mm to 1.4 mm (peak: 1.5 to 3.1 mm).

Correlation calculations in phantom scans showed that the change in tilt angle needed to create uncorrelated images is 4 to 6 degrees. In compounding phantom scans obtained at differential scan angles of 4 degrees, the signal-to-speckle noise ratio (SNR) increased 10% to 20% less than the theoretical $\sqrt{N}$ dependence for N compounded, uncorrelated images. The average misregistration in phantom scans using full affine transformations was 0.21±0.02 mm and did not vary significantly with tilt angle. As a result of misregistrations, the average boundary width of the spheres in a phantom image compounded from 5 scans increased 20% compared to the uncompounded image. In the same compound image, the SNR increased 95%.
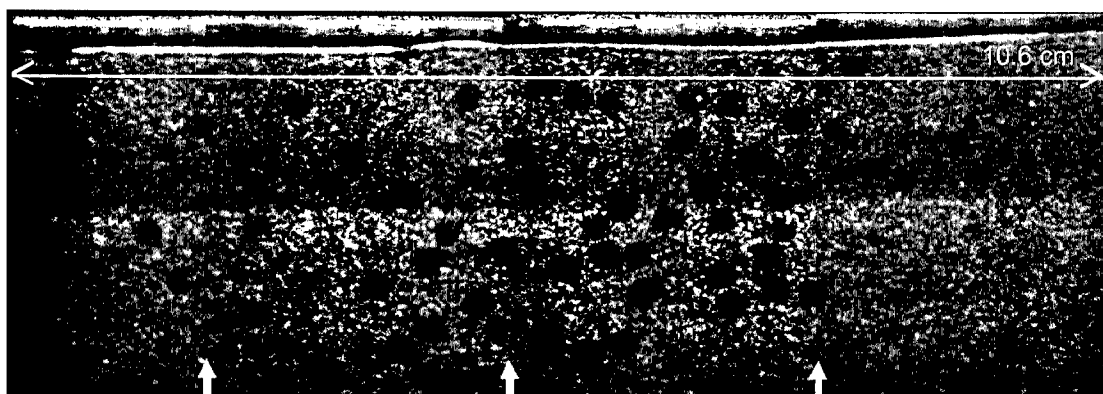

Figure 3: Axial-lateral cross section of an extended volume created from 4 partly overlapping phantom scans.

Figure 4 shows an example of an uncompounded clinical image in breast (a), and the same image compounded from 5 scans at 0°, 6.4°, 12.8°, -5.1°, and −10.2°, using 11 control point warping transformations (b). Statistical analysis showed an almost ideal $\propto \sqrt{N}$ increase in SNR and CNR (contrast-to-noise ratio) for N compounded images. Note the overall reduction in granularity and the better delineation of connective tissues (arrows).

The same data sets were also registered using full affine transformations. Comparing the warped data sets to the linearly transformed sets we found an increase in average estimated misregistration from 0.42±0.10 mm to 0.75±0.12 mm, suggesting that warping can correct for local tissue deformation that is unaccounted for by global linear transformations.

We conclude that image registration is a promising tool in 3-D ultrasound, allowing applications such as accurate extended volume imaging and 3-D compounding. Using image-based registration with non-linear mapping transformations prior to compounding offers the unique potential to correct for tissue motion and refraction artifacts, effects that can greatly distort image quality in other compounding approaches.
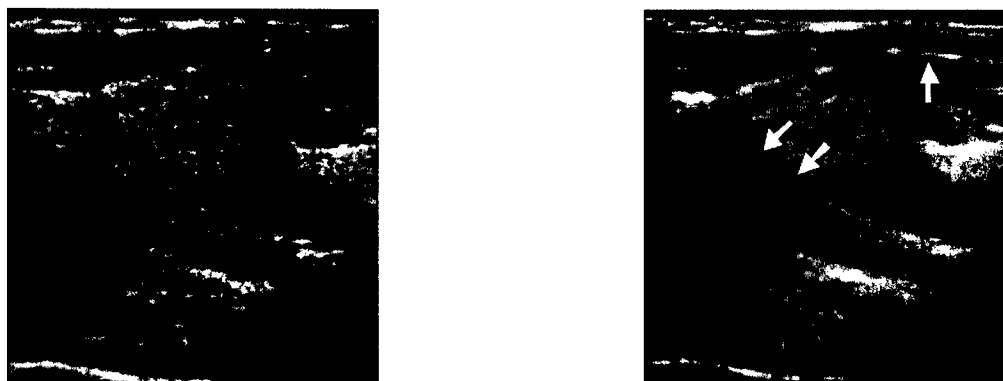

Figure 4: (a) Uncompounded image from reference scan. (b) Same image compounded from 5 scans at 0°, 6.4°, 12.8°, -5.1°, and −10.2°.

ACKNOWLEDGMENTS

REFERENCES

1. Meyer, C.R., Boes, J.L., Kim, B., et al., *Ultrasound in Med. & Biol.* (in press)
2. Rohling, R.N., Gee, A.H., Berman, L., *Ultrasound in Med. & Biol.* **24**, pp. 841-854 (1998)
3. Moskalik, A., Carson, P.L., Meyer, C.R., Fowlkes, J.B., Rubin, J.M., Roubidoux, M.A., *Ultrasound in Med. & Biol.* **21**, pp. 769-778 (1995)
4. Meyer, C.R., Boes, J.L., Kim, B., et al., *Med. Image Anal.* **1**, pp. 195-206 (1997)
5. Krücker, J.F., LeCarpentier, G.L., Meyer, C.R., Roubidoux, M.A., Fowlkes, J.B., Carson, P.L., submitted to *RSNA Electronic Journal* (1999)

Biomedical Imaging Symposium

NIH Office of Extramural Research - OER

Visualizing the Future of Biology and Medicine

June 25–26, 1999

Natcher Conference Center
National Institutes of Health
Bethesda, MD

Charting a vision for the future of biomedical imaging research is the goal of a 2-day symposium presented by the National Institutes of Health with joint support by

AIMBE - American Institute for Medical and Biological Engineering

and
RSNA - Radiological Society of North America.

RSNA

For information, contact:
Chipper Whalan
Capital Consulting Corporation
telephone: 301.468.6001
fax: 301.468.0338
email: bioimaging@md.capconcorp.com
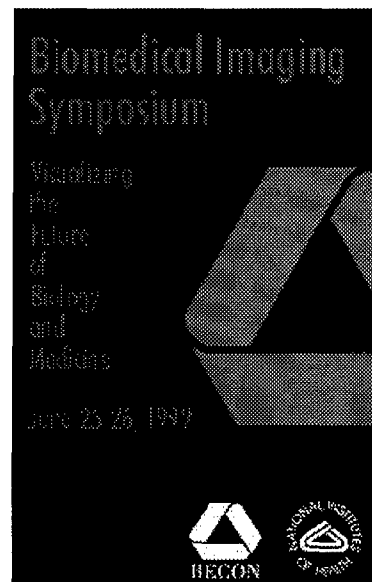
Persons with disabilities who require assistive devices or services to participate in this activity should contact Ms. Whalan to ensure accommodation of their needs.

Note: We have reached capacity for symposium attendance. No further registrations will be accepted online or at the meeting.

web posting: 99/01/12
Webmaster

Abstract:
Diverse developments of 3D ultrasound imaging of the breast and breast lesion vascularity have been undertaken, and increasing promise of characterization of benign versus malignant lesions has been reported. As a notable example, we recently studied a moderate number (38) of women scheduled for breast biopsy and found particular value in Speed Weighted pixel Density (SWD). The technique uses a position-encoding apparatus developed by our group to gather parallel frequency-shift Doppler images (f-CDI) of each volunteer subject. A radiologist then identifies each suspicious mass with a 3D ellipsoid, dynamically positioned and shaped within each reconstructed f-CDI volume. The maximum vascularity (SWDmax) is determined from regions in and around the lesion and is then assessed in conjunction with gray scale (GS) characteristics, which are ranked and averaged. Pathologic findings of this particular group (18 benign, 20 malignant) were used to evaluate our diagnostic accuracy, as demonstrated by receiver operating characteristics (ROC) for SWD and GS as well as combinations of these, with Age, which provided SWD-Age, SWD-GS, and SWD-Age-GS indices. Performance of SWD was comparable to that of the subjective GS, as indicated by the areas under the ROC curves, roughly equal to 0.9 in both cases, where 1.0 describes the perfect discriminator. The two-variable indices enhanced discrimination, while SWD-Age-GS yielded 100% cancer discrimination. The particularly attractive SWD-Age results, given the objectivity of both variables, and the remarkable three-variable results in this patient pool suggest that quantitative vascularity measurements can considerably improve malignant tissue characterization beyond subjective GS evaluation alone.

Introduction:
The relatively non-specific nature of mammography [1] in the early detection of breast cancer has led to a variety of classification schemes to enhance diagnoses [2]. Other imaging modalities such as ultrasound have also been employed to reduce needless biopsies [3,4]. Based on the potential benefits of combining 3D sampling and quantitative vascular assessments, a preliminary study was performed by our group to evaluate which color Doppler ultrasound signals might provide discrimination of breast cancer from benign masses [5]. In a subsequent study, a particular vascularity measure, Speed Weighted pixel Density (SWD) was measured in each of 4 regions of interest in and around suspicious breast masses and compared favorably to standard gray scale criteria [6]. We present here results from the ongoing investigation of this promising discrimination technique.

Methods:
Our subject pool is comprised of volunteer patients with suspicious breast masses scheduled for biopsy. The 38 women presented here were evaluated using a GE Logiq 700 and M12 linear matrix array scanhead (6 MHz Doppler, 9 MHz gray scale). Parallel frequency-shift color Doppler image (f-CDI) slices are obtained at known intervals by translating the transducer while acquiring distance measurements from a linear encoder as shown in Figure 1 above. These image sets are subsequently cropped and reconstructed into 3D ultrasound volumes using a DEC workstation, AVS/Express, and in-house processing software. A radiologist identifies each suspicious mass with a 3D ellipsoid, dynamically positioned and shaped within each reconstructed f-CDI volume. Speed Weighted pixel Density (SWD), defined as the mean velocity times the colored pixel density, is calculated in each of the four volumes of interest shown in Figure 2. The maximum vascularity index (SWDmax) is the

maximum of these four calculations. An example of the radiologist's ellipsoidal definition is shown in Figure 3. Gray scale (GS) characteristics of each mass are also evaluated, ranked on a scale of 1 to 5 (low to high suspicion), and averaged. These include margin smoothness, margin visibility, homogeneity, attenuation, echogenicity, shape, and height. Linear combinations of these values of SWDmax, GS, and patient age give rise to a variety of indices and form the basis of the differentiation of malignant from benign lesions presented here. Pathologic findings are used as "truth" data in classifying a given case as benign or malignant. Discrimination thresholds are determined using a linear Baysian classifier for the two-variable and three-variable cases. In addition, thresholds are determined to minimize false-negative diagnoses. Finally, maximum likelihood estimates of single binormal ROC curves for the indices are calculated to determine their comparative performance. Shown here are comparative results of SWD and GS as well as the multi-variable indices SWD-Age, SWD-GS, and SWD-Age-GS.

Results:
As shown in Figure 3, vascularity is easily visualized from the 3D reconstructed ultrasound volume. Not apparent in a static picture is the ease with which the entire volume can be inspected in three dimensions. The ellipsoid shown was produced during one such session. More quantitatively, Figure 4 shows a relatively "raw" representation of our historically most promising measure of vascularity, log(SWDmax), versus patient age. One can appreciate the discriminating ability of SWD alone by envisioning a horizontal line on the same plot. Also of note is the decrease in vascularity with age (particularly in the benign cases), which makes the two-variable index somewhat intuitive. The diagonal line represents a Baysian discrimination line, equally weighing the cost of false-positive and false-negative diagnoses. Compressing these data into a single index yields the graph shown in Figure 5. Note the reasonable specificity (True Negative Fraction) when the threshold is lowered to produce a sensitivity of 100%. Using a 3D linear Baysian discrimination scheme (which produces a threshold plane), the average gray scale rating (GS) is included in a similar representation of the three-variable index SWD-Age-GS shown in Figure 6. A classification scheme slightly weighted (2:1) to reduce the risk of false negatives produces a threshold discriminator able to completely differentiate between malignant and benign cases. Figure 7 summarizes the diagnostic performance of the various indices with maximum likelihood estimates of receiver operating characteristic (ROC) curves for the indices shown in Figures 5 and 6 as well as the SWD-GS index and the SWD and GS variables alone. As indicated by the area (Az) under each ROC curve, the performance of SWD was comparable to that of the subjective GS [Az(SWD)=0.90; Az(GS)=0.89]. Discrimination is enhanced with a two variable measure, as demonstrated by the SWD-Age and SWD-GS results [Az(SWD-Age)=0.96; Az(SWD-GS)=0.97], while SWD-Age-GS yielded 100% discrimination of cancer. Evaluation of the statistical significance of these recent findings is currently underway. (Comment: I would think that there would be some way to calculate the relative significance (confidence) of a given discrimination value (90% for one variable vs 100% for combining three with a patient population of 38) based on the number of variable added and the number of patients included in the study. Unfortunately I am not sure how this is done statistically. Perhaps Jon Rubin or Paul would know or we can go to the statistical core with it.)

Conclusions:
Vascularity in and around suspicious breast lesions can be quantified and used as an adjunct measure to current diagnostic tests. These vascular measures can be easily combined in a linear fashion with other indicators to produce useful indices. Since the performance of the combined SWD-Age

measure is comparable to the SWD-GS index, it is a particularly attractive, given the objectivity of both the SWD and Age variables. Combining the SWD-Age index with a subjective gray scale rating yields remarkable results, at least in this particular patient pool, and suggests that quantitative vascularity measurements can considerably improve malignant tissue characterization.

References:
1. Sickles EA. Quality assurance: how to audit your own mammography practice. Radiologic Clinics Of North America, Jan;30(1):265-75, 1992.
2. Leichter I, Lederman R, Bamberger P, Novak B, Fields S, Buchbinder SS. The use of an interactive software program for quantitative characterization of microcalcifications on digitized film-screen mammograms. Investigative Radiology, Jun;34(6):394-400, 1999.
3. Stavros AT, Thickman D, Rapp CL, Dennis MA, Parker SH, Sisney GA. Solid breast nodules: use of sonography to distinguish between benign and malignant lesions, Radiology 196, 123-134, 1995.
4. Cosgrove DO, Kedar RP, Bamber JC, al-Murrani B, Davey JB, Fisher C, McKinna JA, Svensson WE, Tohno E, Vagios E, et al. Breast disease: color Doppler US in differential diagnosis, Radiology 189: 99-104, 1993.
5. Carson PL, Fowlkes JB, Roubidoux MA, Moskalik AP, Govil A, Normolle D, LeCarpentier, GL, Nattakom S, Rubin JM. 3D doppler image signal quantification of breast masses. Ultrasound in Medicine and Biology, 24(7), 945-52, 1998.
6. LeCarpentier GL, Bhatti PT, Fowlkes JB, Roubidoux MA, Moskalik AP, Carson PL. Utility of 3D ultrasound in the discrimination and detection of breast cancer, RSNA EJ, 1999, http://ej.rsna.org/ej3/EJ0103-99.fin/abstract.html (accepted).

Figure Captions:

Figure 1. Scanning apparatus. The hand-controlled transducer device is designed to provide guided trajectory of the transducer while measuring linear position and rotation angle. At the base, a linear position encoder is fastened behind a small linear bearing which enables motion in the x-axis, perpendicular to the transducer. An output signal across the encoder is acquired by our computer interface for position registration (resolution = 18 microns). A light weight rotary optical encoder provides angular measurement with a resolution of 0.04 degrees. The patient is scanned through the window in the base plate.

Figure 2. Regions of interest in and around the suspicious mass. A 3 mm shell is computer generated around the radiologist's ellipsoidal estimate of the mass. Our quantitative values are calculated in four regions: (a)* the proximal half of the radiologist's ellipsoid, (b)* the entire ellipsoid of the radiologist, (c)* the proximal half of the shell, and (d)* the entire 3 mm shell.

Figure 3. Example of a radiologist defined ellipsoid. Three ultrasound image planes are shown in the example, highlighted with 3D rendered vascularity in a 55 year old patient with invasive ductal carcinoma with lymphatic invasion. Two of the image planes are reconstructed from the 3D volume. The vascularity is apparent, mostly in the immediate periphery of the ellipsoid.

Figure 4. Discrimination of benign (*) and malignant (*) breast tumors for 38 cases studied: 18 benig (mean age 46), 20 malignant (mean age 56). The plot depicts one of our quantitative vascularity measures, log of the maximum value of Speed Weighted pixel Density (SWD), versus patient age. Using the slope (0.051) of the discrimination line determined by a linear Baysian classifier, a combine SWD-Age index was calculated for each patient and plotted in Figure 5.

Figure 5. Combined SWD-Age Index. Points are spread horizontally for clarity. The upper threshold line shown represents the value of log(SWDmax) at Age=0 of the unweighted discrimination line of Figure 4. This threshold yields a reasonable true positive fraction (TPF) and true negative fraction (TNF) of 0.90 and 0.94, respectively. Requiring a TPF of 1.00 reduces the TNF to 0.56. A similar approach, including the average grayscale rating (GS), produces the SWD-Age-GS index shown in Figure 6.

Figure 6. Discrimination Index including one subjective measure, grayscale rating (GS). As depicted with the upper horizontal line, an unweighted discriminator provides excellent sensitivity (90%) and specificity (100%). Although these data represent only 38 patients, the promising result of complete discrimination (lower threshold line) can be achieved with a Baysian classification scheme slightly weighted (2:1) to reduce the risk of false negatives.

Figure 7. Diagnostic performance of SWD, GS, and Age. The curves shown are maximum likelihood estimates of ROC curves for the indices shown in Figures 5 and 6 as well as a SWD-GS index and the SWD and GS variables alone. As indicated by the area under each curve (Az), the solo performance o our quantitative, objective, measure of vascularity (SWD) is comparable to that of the subjective grayscale rating. Two-variable indices enhance discrimination, as demonstrated by the results of SWD GS and SWD-Age. Adding one subjective variable, GS, to the SWD-Age index yielded remarkable results (at least in this particular patient pool), providing %100 cancer discrimination.
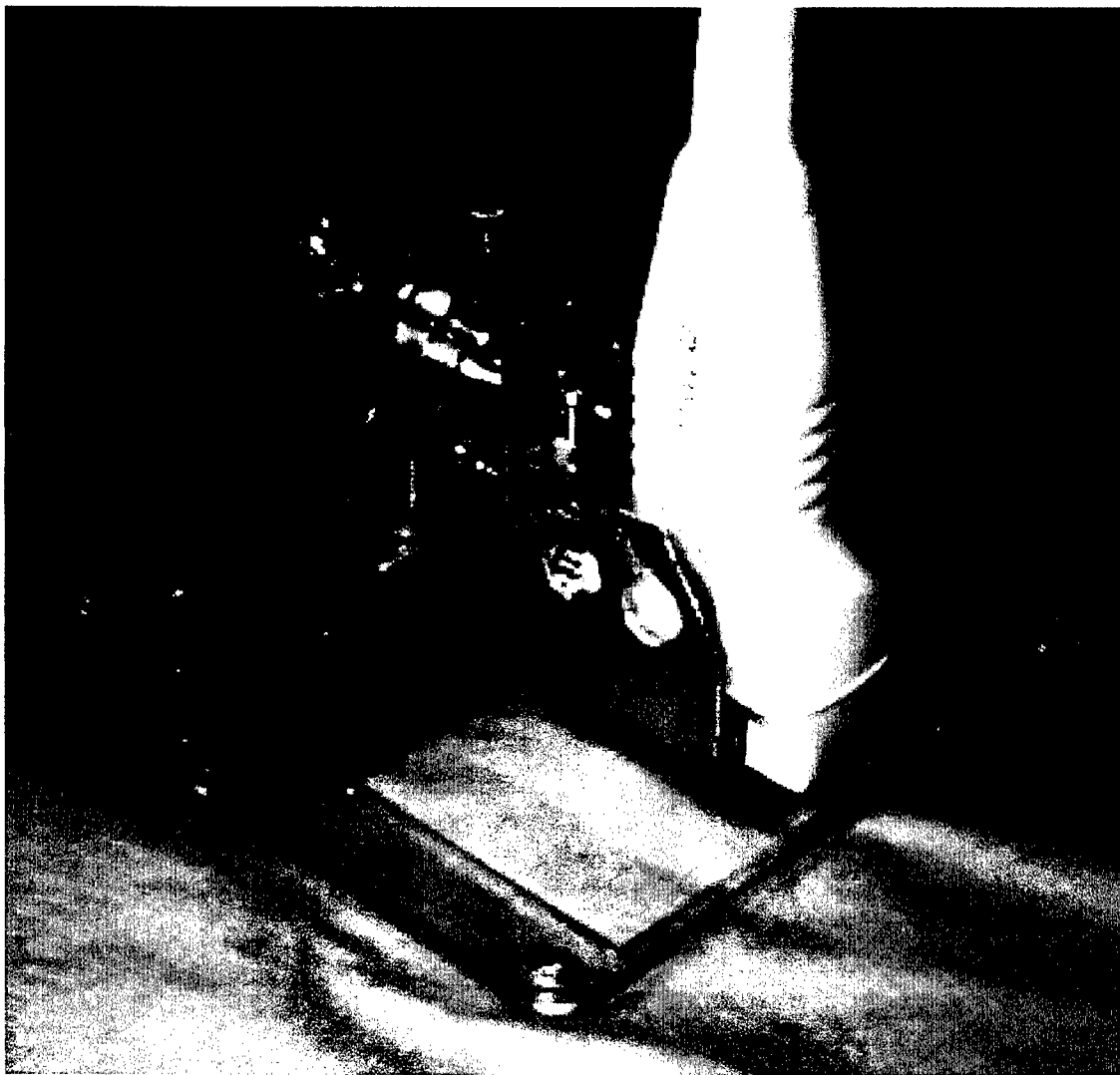
Figure 1. Scanning apparatus. The hand-controlled transducer device is designed to provide guided trajectory of the transducer while measuring linear position and rotation angle. At the base, a linear position encoder is fastened behind a small linear bearing that enables motion in the x-axis, perpendicular to the transducer. An output signal across the encoder is acquired by our computer interface for position registration (resolution = 18 microns). A light weight rotary optical encoder provides angular measurement with a resolution of 0.04 degrees. The patient is scanned through the window in the base plate.
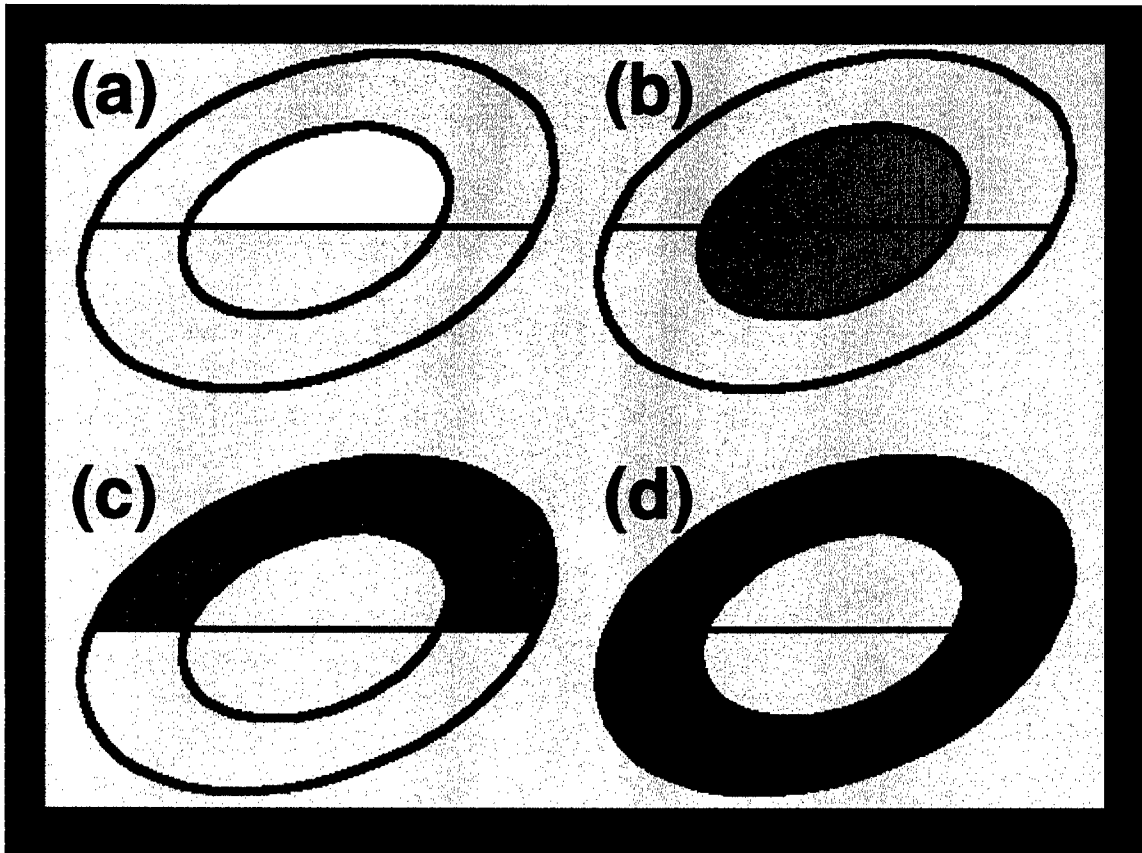
Figure 2. Regions of interest in and around the suspicious mass. A 3 mm shell is computer generated around the radiologist's ellipsoidal estimate of the mass. Our quantitative values are calculated in four regions: (a)* the proximal half of the radiologist's ellipsoid, (b)* the entire ellipsoid of the radiologist, (c)* the proximal half of the shell, and (d)* the entire 3 mm shell.
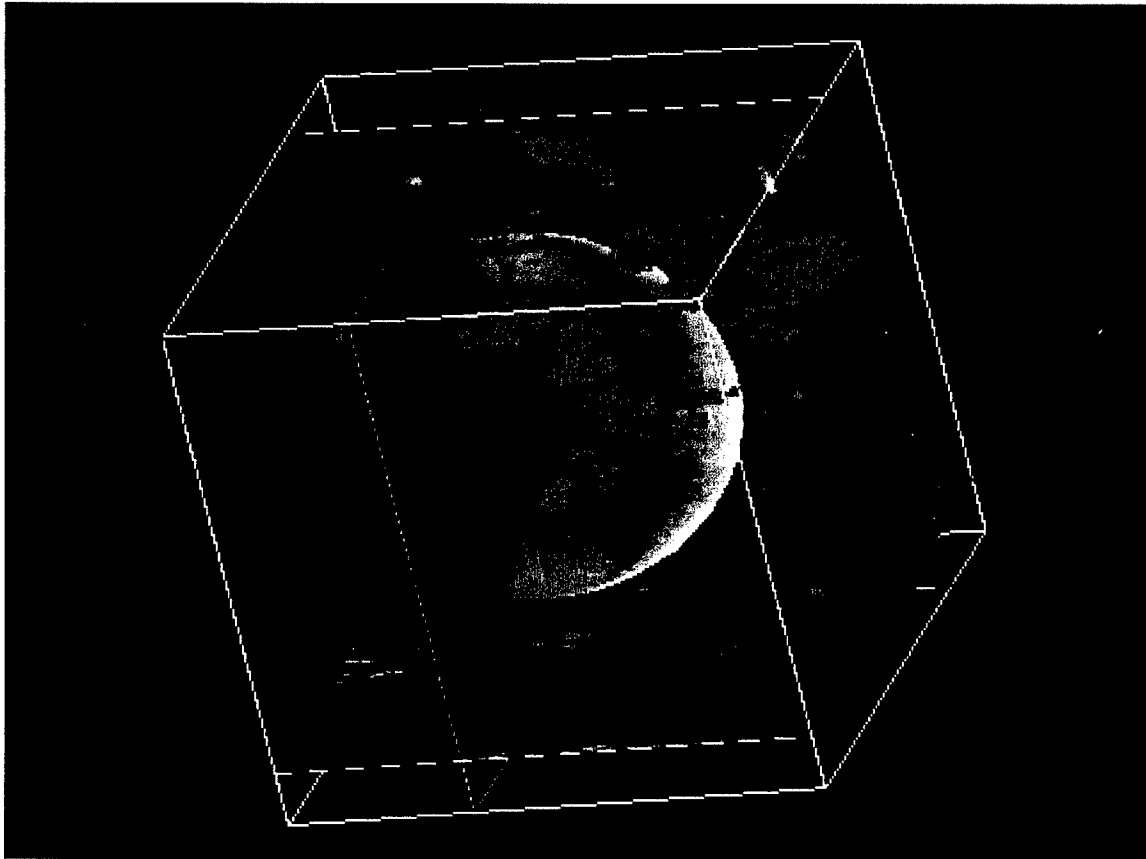
Figure 3. Example of a radiologist defined ellipsoid. Three ultrasound image planes are shown in the example, highlighted with 3D rendered vascularity in a 55 year old patient with invasive ductal carcinoma with lymphatic invasion. Two of the image planes are reconstructed from the 3D volume. The vascularity is apparent, mostly in the immediate periphery of the ellipsoid.
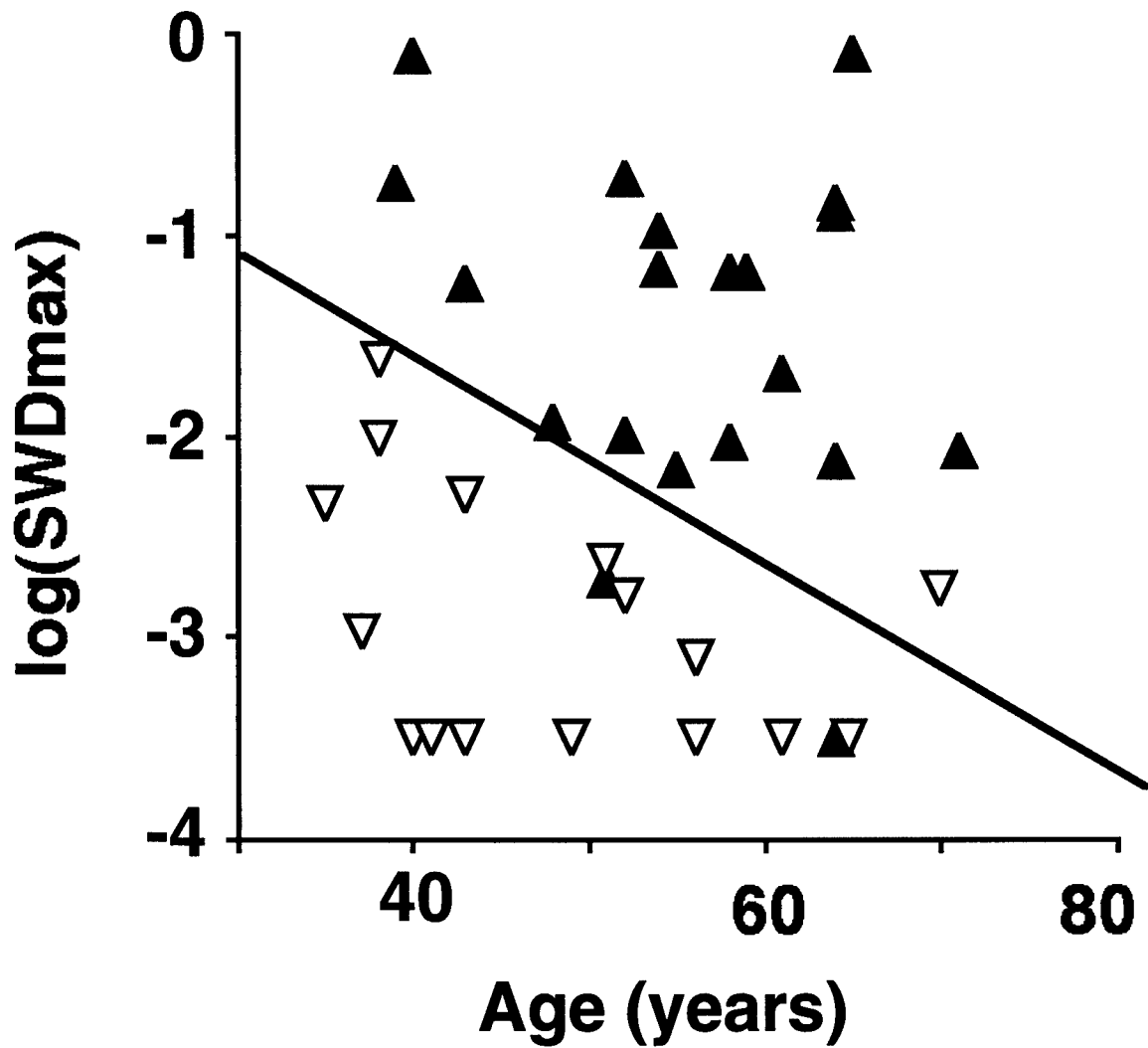
Figure 4. Discrimination of benign (*) and malignant (*) breast tumors for 38 cases studied: 18 benign (mean age 46), 20 malignant (mean age 56). The plot depicts one of our quantitative vascularity measures, log of the maximum value of Speed Weighted pixel Density (SWD), versus patient age. Using the slope (0.051) of the discrimination line determined by a linear Baysian classifier, a combined SWD-Age index was calculated for each patient and plotted in Figure 5.
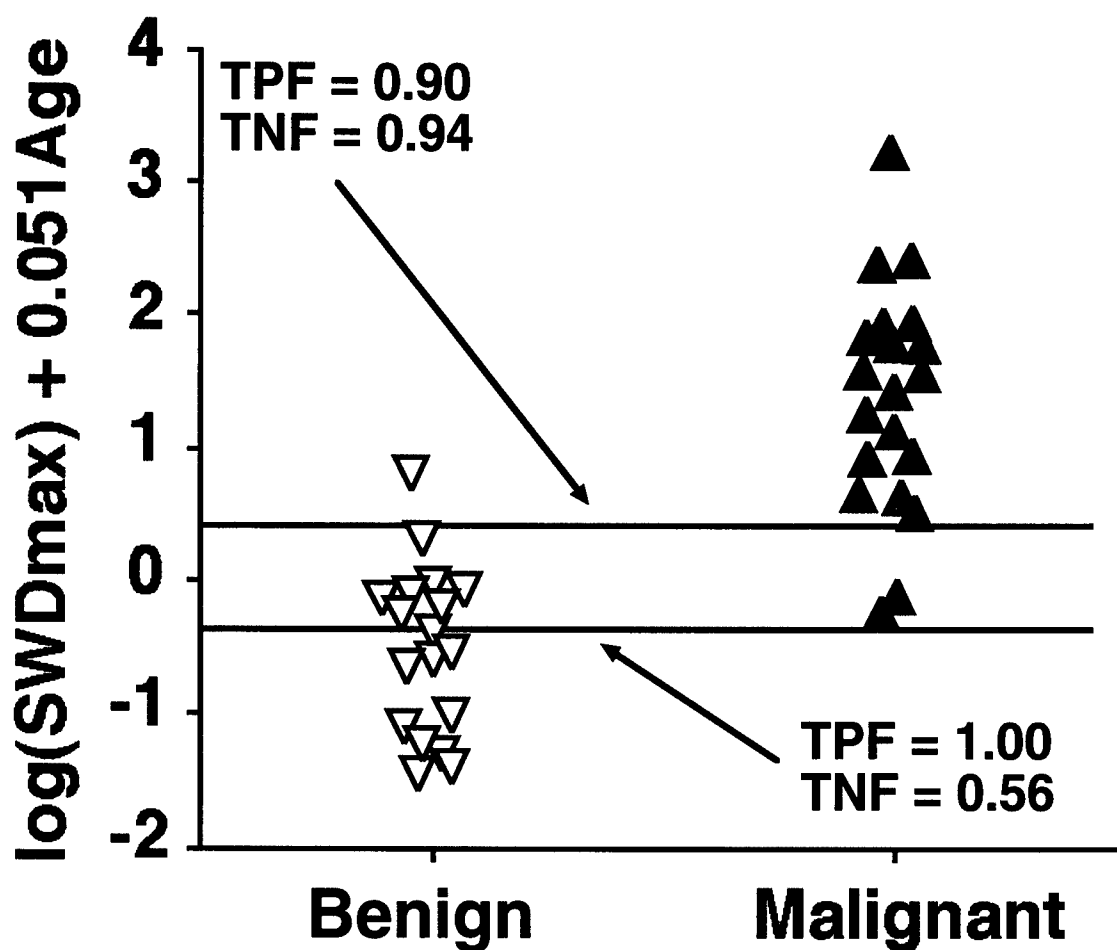
Figure 5. Combined SWD-Age Index. Points are spread horizontally for clarity. The upper threshold line shown represents the value of log(SWDmax) at Age=0 of the unweighted discrimination line of Figure 4. This threshold yields a reasonable true positive fraction (TPF) and true negative fraction (TNF) of 0.90 and 0.94, respectively. Requiring a TPF of 1.00 reduces the TNF to 0.56. A similar approach, including the average grayscale rating (GS), produces the SWD-Age-GS index shown in Figure 6.
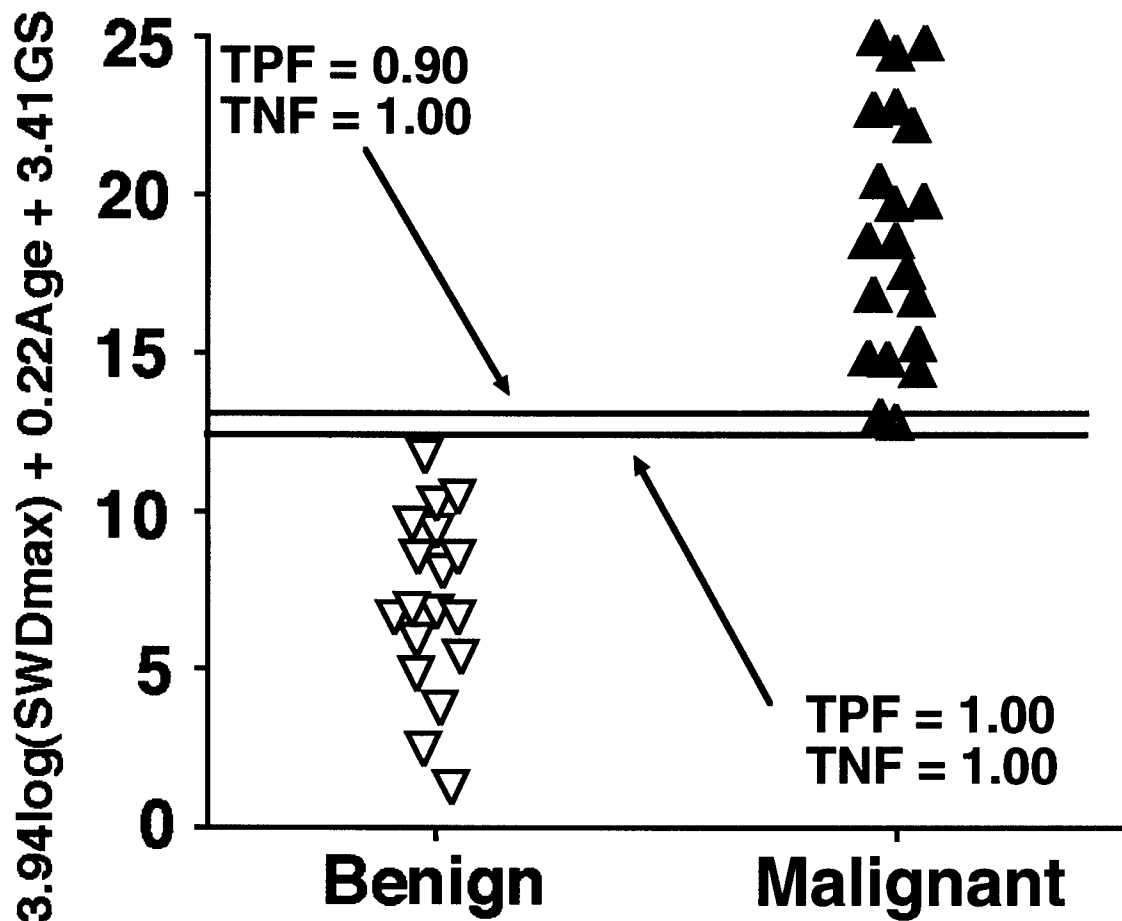
Figure 6. Discrimination Index including one subjective measure, grayscale rating (GS).   As depicted with the upper horizontal line, an unweighted discriminator provides excellent sensitivity (90%) and specificity (100%). Although these data represent only 38 patients, the promising result of complete discrimination (lower threshold line) can be achieved with a Baysian classification scheme slightly weighted (2:1) to reduce the risk of false negatives.
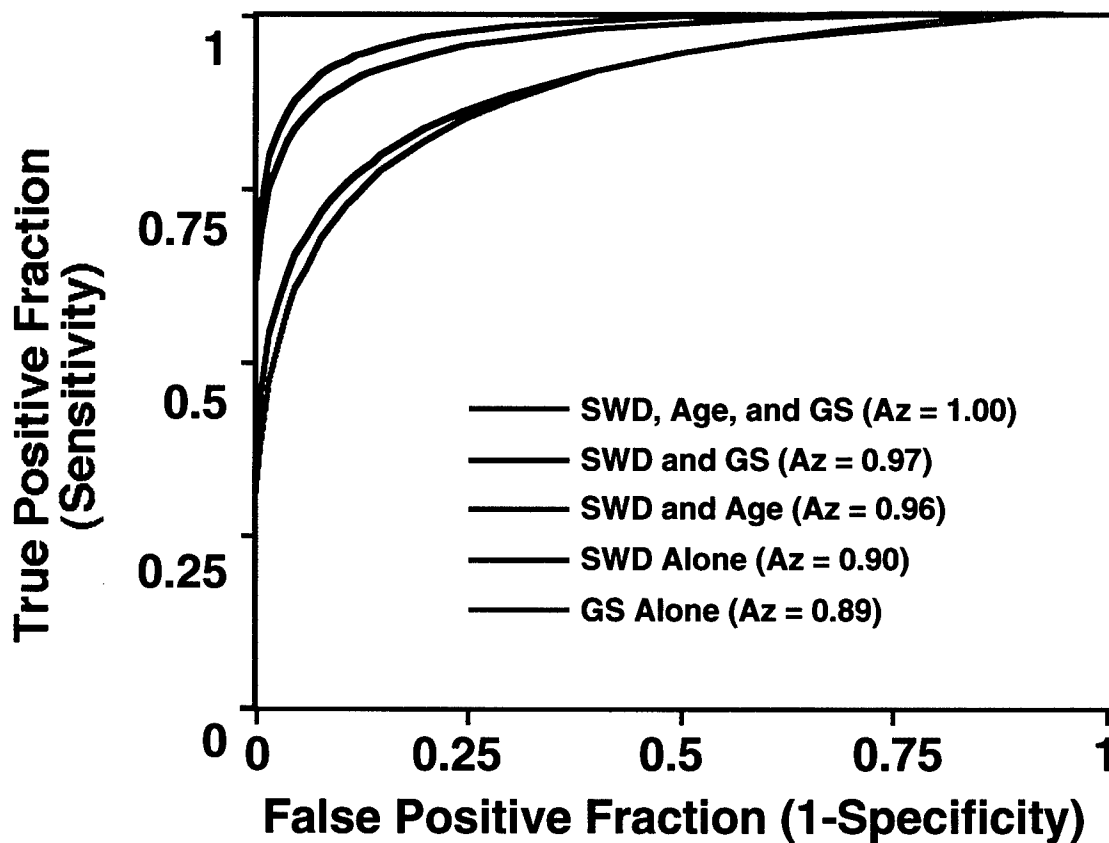
Figure 7. Diagnostic performance of SWD, GS, and Age. The curves shown are maximum likelihood estimates of ROC curves for the indices shown in Figures 5 and 6 as well as a SWD-GS index and the SWD and GS variables alone. As indicated by the area under each curve (Az), the solo performance of our quantitative, objective, measure of vascularity (SWD) is comparable to that of the subjective grayscale rating. Two-variable indices enhance discrimination, as demonstrated by the results of SWD-GS and SWD-Age. Adding one subjective variable, GS, to the SWD-Age index yielded remarkable results (at least in this particular patient pool), providing %100 cancer discrimination.

DEPARTMENT OF THE ARMY
US ARMY MEDICAL RESEARCH AND MATERIEL COMMAND AND FORT DETRICK
810 SCHRIEDER STREET, SUITE 218
FORT DETRICK, MARYLAND 21702-5000

REPLY TO
ATTENTION OF:

MCMR-RMI-S (70-1y)   17 Oct 01

MEMORANDUM FOR Administrator, Defense Technical Information
Center (DTIC-OCA), 8725 John J. Kingman Road, Fort Belvoir,
VA 22060-6218

SUBJECT: Request Change in Distribution Statement

1. The U.S. Army Medical Research and Materiel Command has
reexamined the need for the limitation assigned to technical
reports written for grants. Request the limited distribution
statements for the Accession Document Numbers listed at enclosure
be changed to "Approved for public release; distribution
unlimited." These reports should be released to the National
Technical Information Service.

2. Point of contact for this request is Ms. Judy Pawlus at
DSN 343-7322 or by e-mail at judy.pawlus@det.amedd.army.mil.

FOR THE COMMANDER:

PHYLIS M. RINEHART
Deputy Chief of Staff for
   Information Management

Enclosure